IEEE Access
Multidisciplinary ⋮ Rapid Review ⋮ Open Access Journal

Received December 31, 2019, accepted January 29, 2020, date of publication February 5, 2020, date of current version February 14, 2020.

Digital Object Identifier 10.1109/ACCESS.2020.2971678

Modeling of Insulation Paper Damage in the Assembly of a Solid Slot Winding

BLAZ STEFE[1], (Member, IEEE), AND MARJAN JENKO[2], (Member, IEEE)
[1]Elaphe Propulsion Technologies Ltd., 1000 Ljubljana, Slovenia
[2]Faculty of Mechanical Engineering, University of Ljubljana, 1000 Ljubljana, Slovenia

Corresponding author: Marjan Jenko (marjan.jenko@fs.uni-lj.si)

This work was supported by the European Union's Horizon 2020 Framework Programme under Grant 724188.

ABSTRACT Tight assembly of stator windings with no insulation paper damage is a manufacturing challenge. We evaluate different sets of parts according to the following parameters: magnet wire thickness, stator slot smoothness, length of the straight magnet wire after the slot end, and type and amount of insulation cap at the end of the slot. These parameters have discrete values with small differences between them. The damage criterion is the decrease of the insulation paper breakdown voltage after assembly/disassembly of parts, assembled in a small set of designed experiments. Parameter values, i.e., levels at individual experiments are set by an orthogonal experiment matrix. Repetition of each experiment provides statistical significance. Data analysis shows that the additive model alone is not sufficient due to the high correlation of the parameters' influences. We extend the model to include interparameter influences, which we model by adding a virtual parameter. The extended additive model generates parameter values that do not degrade the insulation paper breakdown voltage within the manufacturing process. These values are verified by repetitions of the control experiment.

INDEX TERMS Analysis of variance, breakdown voltage, design for experiments, design for manufacture, dielectrics and electrical insulation, extended additive model, insulation paper damage, insulation testing, interparameter influence, in-wheel motor reliability, matrices, metal-insulator structures, orthogonal matrix experiments, permanent magnet motors, stators.

NOMENCLATURE

η	Result quality
η_i	Result quality η of the i-th experiment
η_{PL}	Result quality η of the experiment with parameter P at level L
$\eta(A\text{I},B\text{J},C\text{K},D\text{M})$	Result quality η of the experiment with parameter A at level I, B at level J,
C	at level K, and D at level M
Err	Additive model error
FF_P	Fisher factor for the parameter P
m_η	Mean of the result qualities η_i
m_{PL}	Mean of the result qualities η_{PL}
PC	Parameter contribution to result quality η
PDF	Probability density function
SS_T	Total sum of squares, which is the sum of squares over all experiments
SS_P	Sum of squares for the parameter P over all levels
SS_{ERR}	Sum of squares of the error
V_B	Insulation paper breakdown voltage

The associate editor coordinating the review of this manuscript and approving it for publication was Jenny Mahoney.

I. INTRODUCTION

The influence of tight assembly parameters on preservation of the insulation paper breakdown voltage is found and their selection for stator manufacturing of an in-wheel electric motor is reached via designed experiments, modeling, simulation, the development of an extended additive model, and experimental verification.

The promises and challenges facing in-wheel motors are addressed in [1], [2]. These embrace the effect of the additional unsprung mass in the wheels on vehicle dynamics, reliability, performance, dimensioning and integration with brakes, steering and wheels [3], [4]; as well as ride comfort and safety [5].

This work is licensed under a Creative Commons Attribution 4.0 License. For more information, see http://creativecommons.org/licenses/by/4.0/

The most relevant obstacle for the widespread use of in-wheel motors is its unsprung mass [6]. Motors with some tens of kilograms of mass cannot qualify [7], but they can work perfectly elsewhere. We address the torque vs. mass problem in the following way:

a) High slot fill factor of the stator winding,

b) Short winding overhangs and unique patented stacking of the overhangs,

c) Short electromagnetic paths,

d) Use of material up to magnetic saturation,

e) The smallest airgap between the stator winding and rotor magnets, and

f) The most efficient heat transfer from the active material to the cooling system.

Factors a) and b) contribute the most to high specific torque (torque/mass ratio, (Nm/kg)) and to manufacturing complexity. The in-wheel motor has not yet become a mass option for car propulsion, even though it got very close to it in terms of development and marketing. The motor needs to be hollow for mechanical brake inclusion and it needs to operate at highest current density because high torque is mandatory - rotor and wheel rotate at the same speed. We were able to reach excellent specific torque but the motor longevity was not sufficient – mostly because of stator insulation breakdown that occurred at accelerated aging. The insulation breakdown problem within accelerated aging and motor use in test vehicles motivated us to perform the presented research. Our results enabled us to produce reliable motors without stator insulation breakdown.

In the electromagnetic and mechanical design we extensively use finite element method (FEM) and methods of production engineering, as in [8]–[11],which uses FEM to obtain input data for methods of robust engineering that generate material and geometrical data for physical prototyping. Our stator slots are narrower than in [10], and overhangs are shorter than in the difficult-to-manufacture [11]. Each presents an additional challenge for manufacturing of the stator winding. Reference [12] reports on contradictions caused by simultaneous requirements for high torque, low mass, physical strength, nonsaturated magnetics and efficient thermal design. FEM simulations add to material and dimensional optimization, but not to the added value needed for robust manufacturing.

Reference [13] investigates the relation between high torque and the required number of stator slots, aiming for a smaller number of wider slots and higher manufacturing tolerances. The FEM analysis and benchmarking show a clear positive correlation between torque and the number of slots. High torque at fixed motor diameter requires narrow slots and short overhangs. Reference [14] introduces challenges of manufacturing into holistic motor optimization. The goal is modular design for scalable solutions. Reference [14] presents a permanent magnet motor for electric vehicle propulsion, but it is not an in-wheel motor.

In-wheel motor design challenges are, again, low mass and high torque. These call for short overhangs [15], minimizing ineffective volume with losses, and a large number of poles, which are consequently narrow and impose requirements on manufacturing, especially on tolerances and on preservation of stator insulation properties in the manufacturing process.

Stator insulation can deteriorate via many mechanisms. Reference [16] identifies sources of stator insulation deterioration as mechanical, electrical and thermal stresses. Additional sources are environmental moisture, dirt, chemicals and possible overvoltage for inverter-fed machines. These can lead to partial discharges with the potential for further deterioration. In [17] and [18] the designed experiments yield data for the modeling of insulation deterioration. The validity of the resulting insulation life-span model is tested with additional points that have not been used for modeling. These tests confirm the suitability of the model. Thermal stress, which starts the development of microscopic cavities and leads to insulation breakdown, is addressed in [19]. Local hot spots are locations of failure that starts with partial electric discharge and develop over time into voltage breakdown. The development of cavities in insulation is observed through a microscope for aging assessment in [20].

References [21]–[24] analyze recent approaches to monitoring insulation deterioration through real-time analysis of terminal currents and voltages. Assessments at terminals fall within the realm of nondestructive testing even if the result is a breakdown [25]. Evaluations with some disassembly, as we have done in this study, constitute destructive testing. Reference [26] studies insulation lifespan modeling with regression trees. Reference [27] studies the same, but with the addition of random forests. These are appealing alternatives to parametric modeling, but their effectiveness relies on the training set. These methods can illuminate problems with large numbers of somewhat interrelated parameters. References [28] and [29] contribute to the modeling of insulation lifespan through the design of experiments, analysis of variance, and response surfaces. The validity of this derived model is tested with additional measurement. Our work is similar to [28] and [29] in methodology, but we focus on manufacturing-related damage to the insulation paper.

References [30] and [31] put FEM and methods of robust design with the help of an orthogonal experiment matrix (OEM) into perspective – optimization of a permanent magnet motor is performed by FEM. Motor manufacturability, another mandatory component of product design, is the next step. The FEM optimization results are further refined until the final solution is physically sound and manufacturable, i.e., it is robust enough in view of material alterations and anticipated fluctuations of the manufacturing process. Reference [32] further underlines the distinction between the deterministic approach to optimization of product properties, and methods of the robust approach for further production-oriented refinements. Peaks and minimums from mathematical derivations can be sensitive to parameter fluctuations caused by manufacturing. The robust approach is all about inclusion of insensitivity, i.e., robustness relative to material alterations and related fluctuations.

Reference [33] is an example of a 3-step approach to optimization of motor weight: a) FEMs. b) These results are used to generate response surfaces. c) These results are used as inputs to a genetic algorithm that produces the final optimization. Manufacturing issues are not addressed in [33].

OEM and Taguchi's methods of robust design are applied to model energy losses in a finished product in [34], which underlines the potential of the OEM/Taguchi approach for solving a variety of technical problems, as in [30], [35]–[38].

Reference [39] studies magnet wire deformation in a tight slot with FEM simulation. Deformation is plastic at moderate pressure.

References [40]–[42] specify the regulation and the two standards for electrical compliance of in-wheel motors. Insulation must sustain a voltage close to 2000 V throughout its lifetime. This, and [19] and [29] address a potential hesitation of evaluating insulation damage in a range of several kVs while having a motor powered by a 400 V car battery. In our case it was early motor failures that triggered the study of manufacturing induced deterioration of the insulation paper. The breakdown voltage V_B is the criterion.

A. SCOPE OF MECHANISMS, STRESSES AND AGING OF THE INSULATION SYSTEMS IN MOTORS CONTROLLED BY PWM VOLTAGES FROM ELECTRONIC INVERTERS

An in-wheel motor is driven by a 10 – 20 kHz pulse width modulated (PWM) voltage from an electronic inverter. The PWM square wave voltage creates a sinusoidal current in a motor winding. The current frequency and associated motor rotation speed are set as momentarily needed, within the electromechanical capabilities of an inverter and a motor.

The frequency of a 15 kHz inverter is 700 times higher than the rotation frequency of a car wheel at a high travelling speed ($v = 150$ km/h, rim diameter $d = 16$ inches, $\omega_{\text{wheel}} = 2\pi$ 22 rad/s). The ratio of the two frequencies is even higher at lower speeds. The direction of the electric field E in the motor insulation changes every 33 μs ($t = 1/2f$). AC driven motors have similar electric and rotational frequency (the ratio of the two frequencies is defined by the number of poles). A PWM voltage is rectangular with fast transitions (the typical transition duration is approximately 50 ns); the AC sine is a most smooth periodic function.

Inverter manufacturers need short duration of leading and trailing edges of the square wave voltage to reduce power loss in the switching devices (IGBTs, and potentially WBG devices in the future). The resulting sharp edges of the square wave voltage produce voltage overshoots on the interface between different impedances. Such is the case on an interface between a supply cable and a motor. Power reflection occurs. The amplitude of a voltage overshoot depends on the level of impedance mismatch at the interface. The worst case voltage overshoot equals the amplitude of the square wave inverter voltage - a pulse of a double inverter voltage occurs at the start of the stator winding every 33 μs at a 15 kHz PWM voltage. The insulation at the beginning of the stator winding is stressed by both speed and amplitude of the voltage change. Insulation aging and dielectric loss are intensified, compared to AC and DC driven motors. Fast PWM voltage edges intrinsically intensify the potential for partial discharges, compared to the influence of a sine wave AC voltage [43], [44]. This we cannot prevent. Partial discharge effects have been observed even in low voltage motors (400 V) on the turns connected to the phase terminals [45]. Observation of partial discharge effects in resin filled motor internals is not straightforward; computer tomography is used in [46] to visually assess the internal damage.

The insulation system insulates a winding from the stator, the inter-winding turns and the three windings among themselves. An adequate insulation system lifetime is reached if practically no partial discharge occurs – neither between the magnet wire and the stator, nor among the inter-winding turns, nor among magnet wires of the three phases. This is the primary task of the insulation system built from a synthetic layered insulation paper, magnet wire insulation enamels and a resin. The insulation system lifetime in an in-wheel motor should be set at twenty years, in line with lifetime of other non-serviceable car components. Relevant standards do not yet exist. Lifetime is predicted by aging tests. Short time designed experiments can be used to predict the insulation lifetime [47].

Each component of the insulation system is individually challenged. Partial discharges should not take place in any insulation component (insulation paper, magnet wire insulation coating, and varnish). Material surface needs to be resistant to surrounding partial discharges. Thus, modified magnet wires, which were introduced as far back as 1985, contain metal oxides to impart partial discharge resistance to the insulation [45]. Such metal oxide bearing enamel is applied just to the surface coats of the magnet wire. Many magnet-wire manufacturers produce now corona resistant and corona free magnet wire for inverter-fed motors. A recent reference [48] reports modification of enamel with an outer conducting layer. Special enamels for magnet wire insulation are in continual incremental development with the aim of improving the spread of partial discharge resulting charge on the insulation surface to prevent damage.

Reference [49] reports a combination of electrostatic FEM simulations and experimental measurements to assess the risk of partial discharge among the wires of stator windings.

Partial discharge inception voltage (PDIV) is measured and modeled in [50] for a twisted pair of magnet wires surrounded by air as a function of wire diameter, enamel thickness and permittivity. The results are on the conservative side. As such, they can be used in motor design. Short time designed experiments can be used to predict the lifetime of magnet wire insulation, as in [51], [52].

Custom-developed insulation materials have much better insulation properties than the surrounding air. Partial discharges would consequentially first take place in the insulation surrounding air and they would start to degrade the insulation through its surface. Vacuum pressure impregnation (VPI) is used to prevent the influence of air to the most extent.

To remove as much air as possible out of an assembled stator, it is first vacuumed in a chamber (0.1 - 1% of environmental pressure). The electrically active structure is then submerged in resin and afterwards thermally treated. Resin qualities are fitness to the VPI process requirements, high voltage and mechanical breakdown strength, and corona resistance [53]. Resin substitutes air after the VPI process. Success of air reduction is evaluated in a motor production control with a partial discharge measurement system. The achievable PDIV for a low voltage motor, as is an in-wheel motor with a typical supply of 400 V, is about 3 times higher than the supply voltage.

Reference [54] studies the lifetime of electric vehicle motors. When the supply voltage is below the PDIV, the degradation rate associated with partial discharge electrical stress can be neglected. The insulation lifetime is then primarily affected by voltage, frequency and temperature [26]. Insulation aging manifests as embrittlement, cracking, erosion, chemical reactions, etc. Temperature cycling, high temperature and mechanical stress are then the primary causes of aging. Reference [54] suggests that the inverter fed machines should be separated in relevant standards to those that are partial discharge free by design and others that would be liable to become sites of partial discharge activity after a sufficiently long operation time. Such a separation could reduce end user cost in inverter-fed machine qualification.

Reference [55] further addresses the evolution in the standards creation. Emerging PWM standards will provide extended coverage of the insulation system design needs. The focus is on achieving the same amount of reliability for the PWM inverter driven motors as it is yet achieved for the AC driven motors.

Compared to pre-inverter requirements, high switching frequency, sharp transition edges and potential voltage overshoots at transitions of the PWM voltage put a tremendous burden on electric insulation system. A holistic design optimization eases this burden to a manageable extent. Holistic optimization of a PWM voltage driven motor includes, but is not limited to:

a) The cable between the drive and the motor needs to be short (less than a meter). This takes cable / motor impedance mismatch out of the equation. A travelling wave effect, i.e., a transmission line effect is not present at short cables (an electric wave propagates about 10 m in 50 ns).

b) Capacitive component of the stator winding impedance needs to be small. This is needed for a high resonant frequency of the winding. The problem of potential voltage overshoot is then shifted to faster PWM voltage transitions.

c) The insulation system needs to be designed for a PDIV about three times higher than the inverter nominal voltage (two times for a potential worst case voltage overshoot plus a safety margin), if feasible.

d) Stator winding impedance and switching speed of the PWM square wave voltage need to be optimized for no or minimum voltage overshoot at the winding start. The optimization envelope can be differently stretched in each of the design freedom dimensions. Filters can be used to prevent voltage overshoot [56]. Use of multi-level inverters at the cost of added complexity reduces $\mathrm{d}V/\mathrm{d}t$ and the associated electrical stress in the insulation [57], [58]. A feedback loop configuration of a motor and an inverter has been proposed in [15], but has not received recognition due to complexity. Advanced PWM algorithm and difficult to implement modification of inverter output stage are reported in [59]. To our opinion the best approach to optimization is reported in [60], where inverter, harness and motor are simulated as one distributed system consisting of RLC elements and voltage sources. Individual RLC values are adjusted for the prevention of voltage overshoots and ringing. The case study in [60] is an aeronautical application.

Insulation system requirements of an in-wheel motor will get more challenging as battery voltage increases.

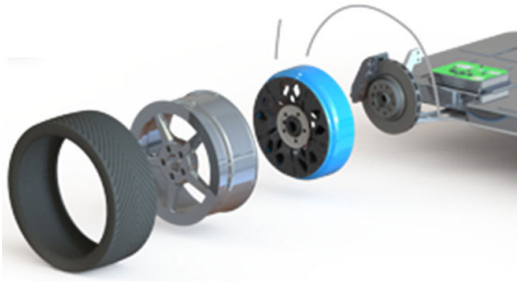

FIGURE 1. Essential components of an in-wheel propulsion system.

FIGURE 2. In-wheel motor for a 15-inch rim, with a maximum torque of 700 Nm.

II. PROBLEM FORMULATION

The essential set-up of components for an in-wheel propulsion system is illustrated in Figure 1.

The components are: the tire, the rim, the in-wheel motor, the disc brake and the inverter. The motor contributes 60 % of the wheel mass. Further mass optimization may require integration of the motor and the rim into one component.

The front and back of the in-wheel motor are shown in Figure 2. The active motor parts – rotary magnets and stationary coils – are positioned around the perimeter of the motor, which provides space for the integration of a mechanical brake. The motor has three phase winding, internal ducts for water-cooling, and angle and temperature sensors that connect to the inverter.

A schematic cross-section of the active region on the motor perimeter is presented in Figure 3.

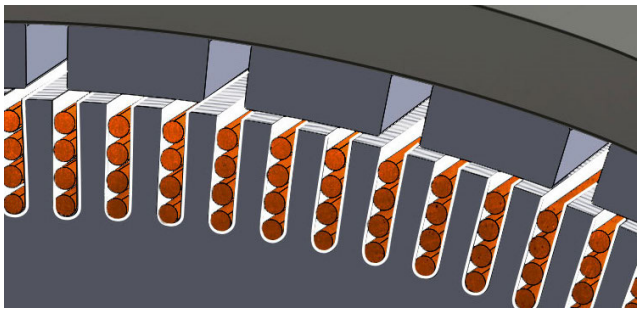

FIGURE 3. Schematic cross-section of the active region on the motor perimeter, the slot width is 2.55 mm.

A stiff magnet wire is inserted into slots. There are four conductors in each stator slot, with the same phase current flowing through each of them in the same direction; three-phase currents flow through windings in sequentially positioned slots. The conductors are rigid and tightly inserted into the stator slots. Neodymium iron boron permanent magnets with alternating orientation are glued to the rotor rim. The design of the motor and its production design complement each other. The goals are high specific torque, reliability and a long lifetime. Properties preservation of the Nomex-Mylar-Nomex (NMN) insulation paper (white slot insert in Figure 3, paper thickness is 0.15 mm) is mandatory throughout the manufacturing process, even though the insulation paper is mechanically stressed during assembly. We have learned by experience that local deteriorations of paper insulation properties, which are induced by mechanical stress, do not always show within test and verification of new motors. The deteriorated insulation constitutes the primary reason for premature motor failures that cannot be repaired because finished stator windings are filled with epoxy resin for adequate heat transfer and protection from dirt and moisture. Manufacturing optimization for the prevention of premature insulation failure triggered our study.

The tight insertion of the stiff magnet wire into stator slots in this motor is essential for a high slot fill factor and better thermal conductance. The magnet wire overhangs must also be short for lower Ohmic losses. Both tight insertion and short overhang result in inevitable mechanical stress on the insulation. We have learned from experience that initial damage reduces motor longevity.

The parameters that have the most influence on degradation of the insulation paper breakdown voltage V_B during assembly are shown in Table 1 and are as follows:

a) Parameter *A*: external diameter of the magnet wire,

b) Parameter *B*: stator slot smoothness,

c) Parameter *C*: length of the straight magnet wire between the end of the stator slot and the start of the curvature,

d) Parameter *D*: type of insulation cap at the end of the stator slot.

To study these parametric influences, we decided on four values, or levels, as indicated in Table 1.

Figure 4a shows the straight magnet wire overhang over stator slot edge, before start of magnet wire curvature.

TABLE 1. Parameters and corresponding levels.

Parameter:	Level: 1	2	3	4
A (mm):	2.38	2.32	2.26	2.20
B (mm):	0.20-0.15	0.15-0.10	0.10-0.05	<0.05
C (mm):	0.00	0.70	1.40	2.10
D, cap:	no insulation	Vitroplast	Nomex	Vitroplast and Nomex

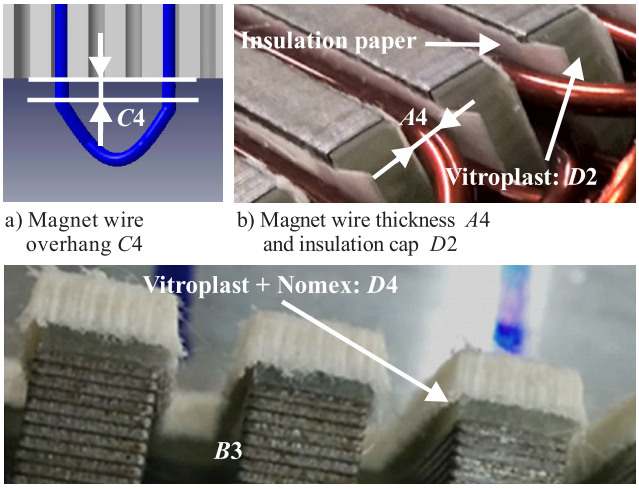

a) Magnet wire overhang *C*4

b) Magnet wire thickness *A*4 and insulation cap *D*2

c) Stator slot smoothness *B*3 and insulation cap *D*4

FIGURE 4. Display of parameters that influence the breakdown voltage V_B of the insulation paper: a) Magnet wire overhang *C*4, b) Magnet wire thickness *A*4 and insulation cap *D*2, c) Stator slot smoothness *B*3 and insulation cap *D*4.

The overhang is annotated with a letter "*C*" since it is parameter *C* in our set of designed experiments. The stiff magnet wire thickness, that is the external diameter of the magnet wire – parameter *A*, the insulation paper, and the optional Vitroplast insulation cap – parameter *D* are visible in the Figure 4b. The optional Vitroplast and Nomex insulation cap, parameter *D*, is in the Figure 4c (dark gray – Vitroplast, white – Nomex). Figure 4c also shows stator slot smoothness – parameter *B*.

The mapping of dimensions and insulation cap material into the parameters level is such that a higher parameter level is expected to suit better in preservation of the insulation paper breakdown voltage V_B. Parameter *A*, the external diameter of the magnet wire, has a diameter ratio of 1 to 0.92 between levels 1 and 4 – this yields a cross-section ratio of 1 to 0.85 – the difference in magnet wire cross section is 15 %. At the same current density this yields a 15 % difference in current *I* between parameter *A* levels 1 and 4. Parameter *B*, slot smoothness – level 1 is produced by a cost-efficient stamping process, and level 4 is produced by expensive precise laser cutting. Parameter *C* – length of the straight magnet wire before curvature results in a 4 % difference of overall magnet wire length between levels 1 and 4. Parameter *D* – insulation cap at the end of the stator slot, results in a 7 % difference of stator cost between levels 1 and 4.

Choosing the parameters level for best/worst torque yields a 1.20/1 ratio, and best/worst stator cost ratio is 0.77/1,

according to the parameters level selection. One would just decide for levels leading to the best case, but definitely not at the cost of decreased reliability resulting in a shorter motor lifetime.

Two other facts need mentioning:

a) The magnet wire insertion needs to be most tight. This works against potential rubbing of the magnet wire caused by forces and vibrations within the motor's lifetime. In principle, the VPI applied epoxy resin mechanically stabilizes the structure, but air bubbles cannot be completely excluded and epoxy resin cannot contribute much to mechanical stiffness. Epoxy resin protects only from environmental influence.

b) The magnet wire enamel consists of a basecoat – polyesterimide with a nominal thickness of 28 μm, and overcoat - poliamide-imide with a nominal thickness of 14 μm. This enamel is not specified as corona resistant. The nominal breakdown voltage V_B of the magnet wire enamel is specified at 7 kV, measured by the IEC 60851-5.4 standard. The nominal breakdown voltage V_B of an NMN insulation paper is specified at minimum 7 kV (spec: 7 kV or more), measured by the IEC 60626 standard. Car batteries operate at 400 V. A combination of inverter's working, motor and cables inductance can produce voltage spikes at up to twice the operating voltage. The required insulation breakdown voltage V_B would be 1500 V after inclusion of a minimal safety factor. The relevant regulation [40] and the standards [41], [42] require sustaining a voltage close to 2000 V throughout the lifetime, which is close to five times smaller than the nominal insulation paper breakdown voltage V_B.

The motivation of this study is not somewhat decreased breakdown voltage V_B of the insulation paper after mechanical stress, rubbing and compressing in assembly of stator parts. The motivation is the prevention of early motor breakdown even as the motor passes production tests. The working assumption was that partial deterioration of insulation paper properties during tight conductor insertion into the slot and narrow conductor bending at the slot edge lead to premature failure of the insulation complex later on in motor exploitation. We chose the breakdown voltage V_B of the insulation paper as a measure of its damage during the assembly of stator parts. The findings of this study confirm the assumption of initial damage of the insulation paper during stator manufacturing. A method for the selection of the optimal parameters level was developed. The result is the parameters level where insulation paper properties are preserved to their full extent within the manufacturing process. Premature failures of the insulation complex no longer occur after allowing for results of this study. Production cost and motor performance are now optimized for reliability. An insight into the ratio of increased torque (current) versus decreased reliability is obtained; for example a motor with 20 % above the specified torque can be built with an expected short lifetime. Such a motor has the potential for e.g., drag racing application. Commercially it is important to demonstrate the highest torque vs. the lowest mass ratio, even for a short duration.

TABLE 2. OEM of parameters *A*, *B*, *C*, and *D* at levels 1...4, where η_i is the result quality from the 1st to the 16th row of the OEM.

A,*B*,*C*,*D* 1...4	η_i	*A*,*B*,*C*,*D* 1...4	η_i	*A*,*B*,*C*,*D* 1...4	η_i	*A*,*B*,*C*,*D* 1...4	η_i
1,1,1,1	η_1	2,1,2,3	η_5	3,1,3,4	η_9	4,1,4,2	η_{13}
1,2,2,2	η_2	2,2,1,4	η_6	3,2,4,3	η_{10}	4,2,3,1	η_{14}
1,3,3,3	η_3	2,3,4,1	η_7	3,3,1,2	η_{11}	4,3,2,4	η_{15}
1,4,4,4	η_4	2,4,3,2	η_8	3,4,2,1	η_{12}	4,4,1,3	η_{16}

Conceptually, dimensional optimization falls along a continuum. Dimensional differences among different parameter levels are relatively small compared to slot dimensions. Expectations for hidden extrema between the discrete material dimensions are about nil.

III. NEW THEORY FOR ASSEMBLY OF A SOLID SLOT WINDING

A. ORTHOGONAL EXPERIMENT MATRIX

To measure the breakdown voltage V_B for all combinations of 4 levels of 4 parameters, a total of 4^4, i.e., 256 experiments are needed. Furthermore, to have a certain amount of statistical significance, each experiment should be repeated 30 times at minimum. Allowing for some extra repetitions, close to 8000 measurements could easily be needed. To keep the amount of experimental work within manageable limits, though, we have structured the combinations of parameter levels into a compact OEM, as shown in Table 2. For each pair of parameters, all combinations of their levels must be represented in such a matrix. This is the only constraint in the construction of the OEM. Structuring experimental work into an OEM of parameter levels is a basic pillar in the Taguchi method of the experiment design for robust manufacturing, [61].

One can structure experimental work into an OEM and induce parameters level for optimal result when the influence of individual parameters on the result is not significantly intertwined. We will investigate the amount of interparameter influence on the result and develop a method to assess its effect in a quantitative term.

From the theory on experiments for robust manufacturing we borrow the term of result quality η. It is defined differently in different types of experiments. In the semiconductor processing industry, for example, η is a logarithmic function of surface defect density [37], [38]. Expressions for η can generally have many forms and they can obfuscate the clarity of OEM properties. The experimenter chooses or defines his own result quality η. In our case the result quality η can simply be equal to the breakdown voltage V_B of the insulation paper. Each of the 16 experiments made by the OEM in Table 2 results in its own insulation paper breakdown voltage V_{Bi} which is equal to our definition of result quality η_i.

The purpose of structuring the experiments into an OEM and analyzing the result qualities η_i is the following:

a) Evaluation of the experimental setup quality, which is high when the result quality η_i depends mostly on the levels of parameters that have been identified as significant. It is low when other parameters (noise) have a significant influence on the result quality η_i. A small standard deviation σ_i of η_i in the 30 repetitions of the unchanged i-th experiment (i = 1 to 16) is a measure of experimental setup quality.

b) Evaluation I of the nature of the experiment set-up. Do the levels (values) of parameters A, B, C, and D define the result quality η interdependently or independently of each other or even somewhat in-between the two distinct options?

c) Evaluation II of the nature of the experiment set-up. Is the result quality η close to a linear function of levels of the parameters A, B, C, and D, or is it a significantly non-linear function?

d) Determination of the parameters level for the best result quality η, which is in our case the same as the highest breakdown voltage V_B.

e) Predicting result quality η for any combination of parameters (A, B, C, D) levels (1, 2, 3, 4).

f) Obtaining data that is qualitatively similar to the measured data of approximately 8000 experiments (256 × 30 + some overhead), from approximately 500 experiments (16 × 30 + some overhead), if this is feasible.

B. MEAN VALUES, 1ST ORDER MOMENTS

After 30 repetitions of each of the 16 experiments with parameter values from Table 1, we assess information in the 16 η_i. Variation of result quality η_i within the 30 experiment repetitions needs to be small enough for statistical relevance. In this case η_i provide a solid base for analysis, which is based on their values. We start the analysis by calculation of means, i.e., of 1st order moments.

The mean m_η of the 16 result qualities η_i is defined by (1).

$$m_\eta = \frac{1}{16}\sum_{i=1}^{16}\eta_i \tag{1}$$

The mean m_{PL} of the result qualities for each level L of parameter P is defined by (2). Four result qualities η_{PL} are needed for each m_{PL} according to Table 2's data.

$$m_{PL} = \frac{1}{4}\sum_{i=1}^{4}\eta_{PL_i} \tag{2}$$

In (2),P stands for parameter – A, B, C, or D, with L being the parameter level: 1, 2, 3, or 4. As an example, equation (3) is (2) written for a case of 4th level of parameter C. Data η_i correspond to experiment indices i in the Table 2 OEM.

$$m_{C4} = \frac{1}{4}(\eta_4 + \eta_7 + \eta_{10} + \eta_{13}) \tag{3}$$

Each m_{PL} is influenced in the same manner by other (not the P) parameters – it is being affected by all 4 levels of any of the other parameters. The OEM structure yields this fact.

One can write (1) as (4), which can then be rewritten as (5):

$$16m_\eta = \sum_{i=1}^{16}\eta_i \tag{4}$$

$$\sum_{i=1}^{16}(\eta_i - m_\eta) = 0 \tag{5}$$

From (5) and (2) one generates (6):

$$\sum_{L=1}^{4}(m_{PL} - m_\eta) = 0 \tag{6}$$

The difference PL between the mean result quality m_{PL} and the overall mean result quality m_η is defined by equation (7):

$$PL = m_{PL} - m_\eta \tag{7}$$

Equation (8) results from (3) and (7):

$$\begin{aligned} m_{C4} &= \frac{1}{4}(\eta_4 + \eta_6 + \eta_9 + \eta_{15}) \\ &= \frac{1}{4}((m_\eta + A4 + B1 + C4 + D1) \\ &\quad + (m_\eta + A3 + B3 + C4 + D4) \\ &\quad + (m_\eta + A2 + B4 + C4 + D2) \\ &\quad + (m_\eta + A1 + B2 + C4 + D3)) \end{aligned} \tag{8}$$

Equations (9) are results of (6):

$$\begin{aligned} A1 + A2 + A3 + A4 &= 0 \\ B1 + B2 + B3 + B4 &= 0 \\ C1 + C2 + C3 + C4 &= 0 \\ D1 + D2 + D3 + D4 &= 0 \end{aligned} \tag{9}$$

Equations (8) and (9) produce (10):

$$m_{C4} = m_\eta + C4 \tag{10}$$

Equation (10) states the same as (7), but it is written for one particular m_{PL}, in this case for $C4$. The objective was to better understand the relationship between the result qualities m_η and m_{PL}.

In the general case we use (11) instead of (10).

$$m_{PL} = m_\eta + PL. \tag{11}$$

When experiments are designed by an OEM, the experimenter would hope that influences of the individual parameters on the result quality η_i in the i-th experiment are independent. Analysis of the particular problem results then confirms or rejects this assumption. In the latter case equation (11) is no longer valid and interparameter influence on the result quality η_i needs to be analyzed. We extend the validity of (11) for an experiment with interparameter influence by inclusion of a currently quantitatively unknown error Err_{PL}. (11) changes to equation (12).

$$m_{PL} = m_\eta + PL + Err_{PL} \tag{12}$$

The error $\mathrm{Err_{PL}}$ is introduced to make (12) valid for any set of η_i data. One part of the error $\mathrm{Err_{PL}}$ can result from the nature of the experiment (influences of individual factors do not just add up, interrelated influences are present). This is a system error. The other part of error $\mathrm{Err_{PL}}$ can result from less than state-of-the-art experimental work. This is experimental error.

Equation (12) is extended into (13) for inclusion of all four factors that contribute to the η value. Result quality

$$\eta\,(A\mathrm{I}, B\mathrm{J}, C\mathrm{K}, D\mathrm{M}) = m_\eta + \mathrm{AI} + B\mathrm{J} + C\mathrm{K} + D\mathrm{M} + \mathrm{Err}. \quad (13)$$

In (13), AI, BJ, CK, and DL are individual contributions of parameter P (A, B, C, D) being set at level L (I, J, K, M) to the experiment quality η. Error Err results from use of the additive model in experiments with some interparameter influence on the result quality η. One hopes for small error, but its' size completely depends on the nature of the physical experiment. For (13) to be useful for experiment analysis, the contributions of individual parameters need to be almost independent of each other. If they are totally independent, their individual influences just sum up to the result and error Err is zero. This is a somewhat simplified model of the real world. In certain cases, such modeling is close enough to a physical situation, while in others it is not. Because the additive model simplifies analysis it is used in many disciplines. For example, superposition in circuit theory and in control systems is based on additivity. With our experiments we assume the property of additivity, or at least being not too far from additivity. Findings in the next section will answer when and how we can use the additive model in our case.

C. ANALYSIS OF VARIANCE, 2ND ORDER MOMENTS

The assessment of problem optimization with moments of 1st order (equations (5) and (6)) constitute the basis for the use of the additive experiment model (13). To trust the results derived from the model, one must confirm the validity of the assumption of parameter inter-independence. Variances – 2nd order moments – will provide the necessary information. Analysis with the help of variances is known as ANOVA.

Variance σ^2, a measure of data scattering, is written in (14) in a form that resembles (5):

$$\sum_{i=1}^{16} (\eta_i - m_\eta)^2 = \mathrm{SS}_T = 16\sigma^2 \quad (14)$$

Variance σ^2, a measure of data scattering, is written in (15) in a form that resembles (6):

$$\sum_{\mathrm{L}=1}^{4} (m_{\mathrm{PL}} - m_\eta)^2 = \mathrm{SS_P} = 4\sigma_P^2 \quad (15)$$

Analysis of the 16 experiments in Table 2 with variance σ^2 has the following purposes:

a) To provide an educated answer as to whether the assumption of the inter-independence of parameters influencing the paper breakdown voltage V_B is correct.

b) If parameter influences are interdependent, upgrading the additive analysis for such modeling.

c) Ranking parameters by their impact on the paper breakdown voltage V_B.

d) The prediction of matching between the calculated maximal V_B and the measured maximal V_B of the insulation paper – both obtained at the best parameters level. For the second V_B, a physical control experiment will be produced and repeated enough times for statistical significance of the measured V_B.

1) EVALUATION OF THE ASSUMPTION ON INTER-INDEPENDENT PARAMETER INFLUENCES ON THE PAPER BREAKDOWN VOLTAGE V_B (CORRECTNESS OF THE USE OF THE ADDITIVE MODEL)

The variance of 16 result qualities η_i is caused by varying parameter levels among 16 experiments organized into the OEM in Table 2. When varying levels of one parameter P only, the variance σ^2 results from σ_P^2, which is written as:

$$\sigma^2 = \sigma_P^2 \quad (16)$$

Equation (16), with the help of (14) and (15), leads to (17):

$$\mathrm{SS_T} = 4\mathrm{SS_P} \quad (17)$$

Assuming interparameter independence one can write (18).

$$\mathrm{SS_T} = 4\mathrm{SS_A} + 4\mathrm{SS_B} + 4\mathrm{SS_C} + 4\mathrm{SS_D} \quad (18)$$

There is no mechanism that would guarantee validity of equation (18) for any results of experiments in the OEM.

The introduction of error, formulated as the sum of squares of error ($\mathrm{SS_{ERR}}$) modifies (18) into (19) which is valid for any measured data. Inclusion of this error adjusts what is needed to balance the potential inequality.

$$\mathrm{SS_T} = 4\,(\mathrm{SS_A} + \mathrm{SS_B} + \mathrm{SS_C} + \mathrm{SS_D} + \mathrm{SS_{ERR}}) \quad (19)$$

Equation (18) is valid when the influences of parameters A, B, C, and D on the result quality η are independent of each other. When not, then the introduction of $\mathrm{SS_{ERR}}$ is mandatory. $\mathrm{SS_{ERR}}$ can be smaller or larger, which is related to the nature of the problem and to the set-up of the experiments.

The ratio between the individual parameter $\mathrm{SS_P}$ ($\mathrm{SS_A}$, $\mathrm{SS_B}$, $\mathrm{SS_C}$, $\mathrm{SS_D}$) and the cumulative influence of all parameters $\mathrm{SS_T}$ - $4\mathrm{SS_P}/\mathrm{SS_T}$ is a measure of individual parameter influence on the experiment's result i.e., on the result quality η. $4\mathrm{SS_{ERR}}/\mathrm{SS_T}$ is a suitable measure of the inadequacy of additive modeling for the specific problem and for the specific experimental work.

2) LOW $\mathrm{SS_{ERR}}$, FISHER FACTORS AND CONFIDENCE INTERVAL

The suitability of the additive approach (13), (19) can be systematically addressed by comparing parameter contributions to the change of result quality η - breakdown voltage V_B. In particular, comparing the contribution of the parameter P change to the corresponding quantity derived from $\mathrm{SS_{ERR}}$.

1st order moment analysis - means and corresponding derivation, gave us (13) but left us with no means to quantify the size of error Err at arbitrary choice of the parameters level. The confidence interval for the calculated result quality η at the certain parameters level is based on the size of SS_{ERR}.

To get from sums of squares SS to assessment of a result change at a certain parameter change, compared to the somehow normalized SS_{ERR}, one introduces degrees of freedom (DF) for a) the OEM, b) for the parameter P and c) for the error Err, which is numerically represented by SS_{ERR}. DFs are defined in relation to means – equations (1) and (2).

The OEM has 16 experiment results η_i with mean m_η. For a known mean, 15 results can vary and the 16th result quality η_{16} is fixed for preservation of the mean m_η. The system of equations thus has 15 DFs.

The sum of influences of each of the parameters (A, B, C, D) at all four possible levels (1. . .4) on the result quality η is 0, by (6). The influences of three parameter levels can vary and the influence of the fourth parameter level is adjusted for preservation of the sum of the four different influences at 0. Each of the four parameters in Table 2 thus has three DFs.

Equation (20) yields the DF for the error.

$$DF_{System} = DF_A + DF_B + DF_C + DF_D + DF_{ERR}, \quad (20)$$

where DF_{ERR} equals 3.

One can then define Fisher factors and error variance. The Fisher factor is a measure of parameter change impact on the result quality η change, compared to the comparable value induced from SS_{ERR}. Equation (21) defines the Fisher factor FF_P for the parameter P.

$$FF_P = \frac{SS_P}{DF_P} \Big/ \frac{SS_{ERR}}{DF_{ERR}} \quad (21)$$

The error variance is defined in (22):

$$\sigma^2_{ERR} = \frac{SS_{ERR}}{DF_{ERR}}. \quad (22)$$

68 % and 95 % confidence interval for the result quality η are derived from (22).

It is important for the validity and relevance of the experiment that Fisher factors (21) be (quite) larger than 1. The effect of a parameter level change is to be larger than the correspondingly scaled error of the additive model. A well-known analogy to these findings is signal-to-noise (S/N) ratio in electrical engineering, control theory, and manufacturing engineering, where the signal level needs to be substantially above the noise level.

3) HIGH SS_{ERR}, LOW FFS: ACCOMODATION OF THE ADDITIVE MODEL TO INTERPARAMETER INFLUENCE ON RESULT QUALITY η

High SS_{ERR} and low Fisher factors are signs of missing contributor(s) to SS_T. The higher is SS_{ERR}, the less is the additive-only model suitable for the particular experiment analysis. High SS_{ERR} results in low Fisher factors – S/N ratio in such an experiment set-up is low. High SS_{ERR} results in high error variance (22), which results in a wide confidence interval of the result quality η – uncertainty of the result quality η is increased. Very high SS_{ERR} renders measured values inadequate for induction of any functional results. Practically, high SS_{ERR} demands restructuring the experiment set-up for a higher S/N ratio between controlled and uncontrolled experiment parameters. Such an undertaking can be most challenging. The time for experiment improvement runs out fast since already the initial experiment set-up had to be made the best possible.

A high SS_{ERR} is a sign of interparameter influence on the result quality η. The OEM in Table 2 can be read as a system of 16 linear equations where:

$$\eta_i = \sum_{j=1}^{4} PC_j \quad (23)$$

In (23), PC stands for the contribution of parameter (A, B, C, D) at a certain level (1, 2, 3, 4) to the result quality η_i. Table 2's OEM can represent a system of 16 linear equations with 16 unknowns, which is solvable. In the case of interparameter influence on the result qualities η_i the 16 equations include parameter cross factors. The mapping of Table 2's OEM into equations as (23) is no longer valid. In such a case an attempt to solve Table 2 data in equations as (23) reports an inconsistent system with no solution. The 16 equations need to be more flexible than just linear with 16 unknowns. They need to include more DFs to take into account the cross factor effects.

The DF of the equation system induced from Table 2's OEM is 15, according to preservation of the mean m_η (1). Addition of DFs to individual equations will increase their capability to match the 16 measured results. Related to preservation of the mean m_{PL} (2), the 4 factors with 4 levels each cumulatively accommodate 12 DFs. Instead of granting the difference of 3 DFs to DF_{ERR} - equation (20), we propose adding a 4-level factor to each of the 16 η_i equations. We name it a virtual factor. Its role is to accommodate cross-factor contributions to result qualities η_i. In terms of calculus it is on a par with the 4 physical parameters. Table 2 is converted to Table 3 by introduction of a 4-level virtual parameter E. It serves as a contributor of cross-factor effects to result quality η.

The DF of each of the 16 equations is equal to DF of the set of the 16 equations. The Table 3 OEM has a) real solutions for any set of the 16 random result qualities η_i, and consequentially, b) the 5 SS_P always sum up exactly to the SS_T: the variance of 16 results is the sum of 5 contributions - variances produced by level changes of each of the 5 parameters. This is explained in more detail in [62] and confirmed by the author's extensive simulation of the OEM in Table 3 (with approximately half a million sets of 16 random result qualities η_i).

A hypothetical inclusion of a 6th parameter (for arbitrary reason) is not possible with the Table 3 OEM since all possible orthogonal combinations are exploited with the 5 4-levels

TABLE 3. OEM of parameters *A, B, C, D, and E* at levels 1...4,η_i is result quality from the 1st to the 16th row of the OEM.

A,B,C,D,E 1...4	η_i	*A,B,C,D,E* 1...4	η_i	*A,B,C,D,E* 1...4	η_i	*A,B,C,D,E* 1...4	η_i
1,1,1,1,1	η_1	2,1,2,3,4	η_5	3,1,3,4,2	η_9	4,1,4,2,3	η_{13}
1,2,2,2,2	η_2	2,2,1,4,3	η_6	3,2,4,3,1	η_{10}	4,2,3,1,4	η_{14}
1,3,3,3,3	η_3	2,3,4,1,2	η_7	3,3,1,2,4	η_{11}	4,3,2,4,1	η_{15}
1,4,4,4,4	η_4	2,4,3,2,1	η_8	3,4,2,1,3	η_{12}	4,4,1,3,2	η_{16}

parameters. Where there are only 3 physical parameters, 2 virtual parameters would have to be added; for 2 physical parameters it would be 3 virtual parameters for $SS_T = \sum_{i=1}^{5} SS_{Pi}$. When so, SS_{ERR} equals 0, which is reflected in a confidence interval of 0. The result quality η becomes a firm value instead of a value with confidence interval.

Two things remain. Calculation of *P*L by (7) produces values for contributions of 4 levels of any parameter, including the virtual parameter *E*. As one calculates result quality η according to the parameters level, the physical parameter level is known. Which level of the virtual parameter matches the set of the physical 4? The decision is made by insight into the physical nature of the experiment, not by calculation. In insulation paper damage, a case with the most damage would get even worse because of parameter interactions, while the least damage should pass with the least parameter interactions.

The last remaining issue is mapping the distribution of 30 repetitions of each of the 16 experiments into the distribution of calculated result quality η for best case, and for any other case. We address this issue by recalculating the equations a statistically significant number of times, where 16 result qualities ηi are scattered with different distributions. After a sufficient number of simulation runs we observe the distribution of the calculated best result quality η.

The best parameters level and the value of the corresponding result quality η are determined by calculation. Simulation of input data scattering adds the η distribution and scattering induced confidence interval around the calculated best or any other result quality η.

D. PREDICTION OF RESULTS

1) BEST RESULT

The expected highest quality of paper insulation is at the highest breakdown voltage V_B, which is the same as the highest result quality η_{MAX} calculated at the best parameters level. Equations (13) and (7) lead to (24) and (25):

$$\begin{aligned}\eta_{MAX} &= m_\eta + \left(m_{AL_{BEST}} - m_\eta\right) \\ &\quad + \left(m_{BL_{BEST}} - m_\eta\right) + \left(m_{CL_{BEST}} - m_\eta\right) \\ &\quad + \left(m_{DL_{BEST}} - m_\eta\right) + \mathrm{Err}, \qquad (24)\\ \eta_{MAX} &= m_\eta + \left(m_{AL_{BEST}} - m_\eta\right) \\ &\quad + \left(m_{BL_{BEST}} - m_\eta\right) + \left(m_{CL_{BEST}} - m_\eta\right) \\ &\quad + \left(m_{DL_{BEST}} - m_\eta\right) + \left(m_{EL?} - m_\eta\right). \qquad (25)\end{aligned}$$

We use (24) when Fisher factors are high (low SS_{ERR}) and (25) for articulated inter-parameters influences (low Fisher factors, high SS_{ERR}).

In (24) and (25) the mean m_η is calculated by (1); the means m_{PL} are calculated by (2).

The size of error Err is unknown in (24). We encapsulate this fact into the η_{MAX} uncertainty range or confidence interval, derived from (22) as (26).

$$\pm 95\%\text{conf. interval} = \pm 2 \text{ std. dev.} = \pm 2\sqrt{\sigma_{ERR}^2} \qquad (26)$$

In (25), the nature of the particular experiment defines the most proper choice of virtual parameter *E*s' level L – which contributes interparameter effects.

2) DECREASED V_B RESULT

To determine the breakdown voltage V_B and result quality η_{ARBIT} for an arbitrary combination of a parameters level, one only modifies levels L_{BEST} to L_{ARBIT} in (24) and (25).

E. SIMULATION

In parallel with developing an experimental concept and building an understanding of the relationship between a parameters level and the result quality η - breakdown voltage V_B, we have developed a simulator of equations to study the effects of different input data, to test independent data influence using the additive model, and interrelated data influence for high errors and low Fisher factors. Most screen-copies of simulator graphical user interface (GUI) windows are available for download of a zipped file from [63]. The program itself is also in [63]. We wrote this simulation tool in C++ Builder, a rapid application development environment. The program consists of approximately 4000 lines of C++ code. Its user interface builds on functionality of the visual component library.

The purpose of making this tool was first to study and then to become confident with the concepts by evaluating them with different input data – for mutually independent, dependent and almost negligibly dependent contributions of the 4 factor levels to the result quality η. The sum of squares SS_{ERR} equals 0 with mutually independent data, growing proportionally with the mutual dependency of parameters. The Fisher factors FF_P get smaller at higher SS_{ERR} values – the suitability of the additive model is lower at increased interparameter influence on result η. Addition of the virtual parameter *E* adds DFs to the 16 OEM equations. Upgrade of the Table 2 OEM to the Table 3 OEM makes $SS_{ERR} = 0$ at any input data.

Verifying the analytical approach with simulation helped to avoid potential mistakes, which would not produce completely wrong results but would introduce difficult-to-note offsets of some scale.

IV. DATA GATHERING

A. STATOR ASSEMBLY

Figure 5 shows a machine for the experimental assembly of stator windings. We measured the pressure and rate of magnet

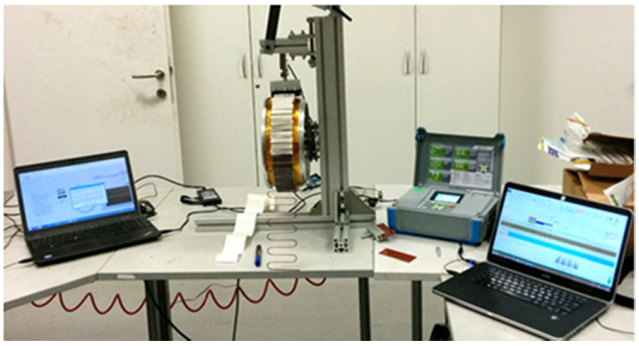

FIGURE 5. A machine for the experimental assembly of stator windings.

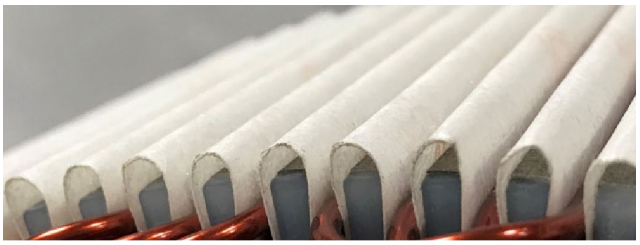

FIGURE 6. Experimental stator assembly with a continuous insulation.

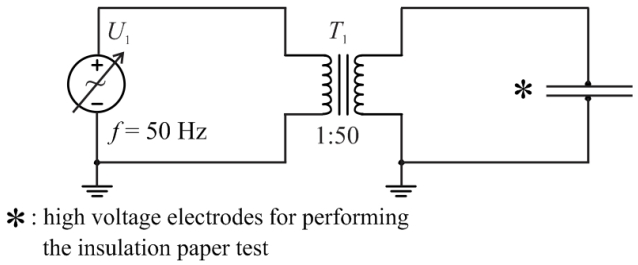

FIGURE 7. Schematic of the system for measuring the AC breakdown voltage of the insulation paper V_B.

wire insertion into the slot and learned that these values do not have an observable influence on the potential degradation of result quality η, which is the insulation paper breakdown voltage V_B.

Figure 6 shows upper part of the experimental stator assembly. The inserted insulation paper is not cut at top of stator slots, as is done in production. The reason is that edge effects would make it impossible to obtain uniform electric field E through the sample. Keeping the stripes together as a sheet of paper eliminates edge effects in measurement. The complex is disassembled after assembly. The insulation paper is put between the HV electrodes for measurements of the breakdown voltage V_B, Figures 8, 9, and 10.

Such an investigation of the insulation paper breakdown voltage V_B is a destructive method, since it is only by disassembling the stator winding that we are able to assess the local deterioration of the insulation paper during the manufacturing process. The forces on the insulation paper are an order of magnitude smaller during disassembly than during the assembly process.

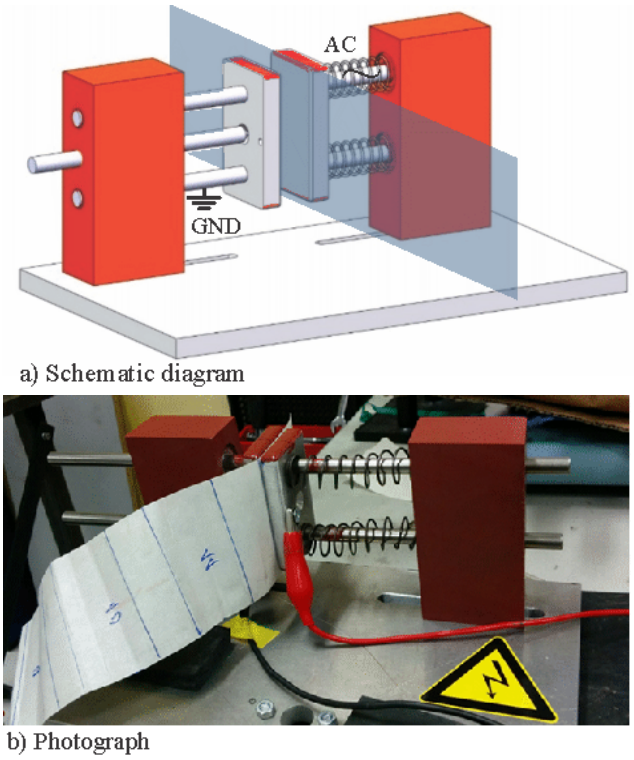

FIGURE 8. High-voltage electrodes for performing the insulation paper test: a) Schematic diagram, b) Photograph.

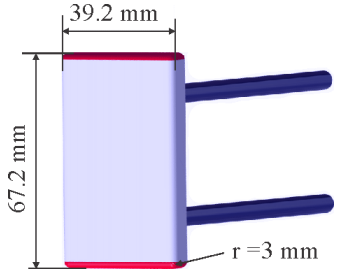

FIGURE 9. A 3D drawing of one of the two HV electrodes.

B. MEASUREMENT OF THE BREAKDOWN VOLTAGE V_B

The measurement is based on the IEC 60243-1 standard for determination of the breakdown voltage V_B with tests at power frequency. The standard recognizes the breakdown voltage V_B as useful data for detecting changes, which are beside others due to different levels of material processing parameters and other manufacturing situations. The standard allows for different implementations, where the results may not be directly comparable, but each implementation may provide useful information on the achievable electric field strength E, and on the breakdown voltage V_B of the investigated material.

Figure 7 shows the essential schematic of the system for measuring the breakdown voltage V_B of the insulation paper. The voltage source U_1 is a motorized control variac. The voltage on the high voltage electrodes is linearly increased at a rate of 500 V/s. Most breakdowns occur between 5 and 10 kV,

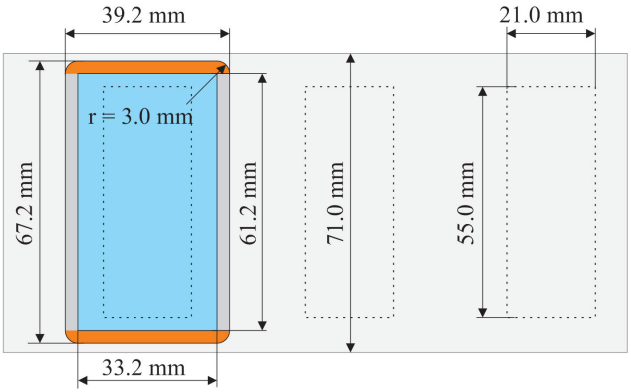

FIGURE 10. Outline of the HV electrode under (or over) the tested insulation paper and of the insulation paper.

which is in time between 10 and 20 s. The standard specifies 5 consecutive tests in quality control measurements. The standard requires more tests for other purposes. We decided for 30 tests in the paper damage assessment measurement.

We follow the standard with the curvature radius of 3 mm, Figures 9 and 10, but none of the electrodes in the standard is applicable to the geometry of our samples.

We also adhere to the IEC 60212 ambient terms: specimens are conditioned and experiments are performed at room temperature and at a relative humidity around 50%.

The outline of the HV electrode, covered with the tested insulation paper is shown in Figure 10. The paper in the 3 dotted-edge rectangles in Figure 10 was installed in 3 consecutive stator slots. The blue area in Figure 10 is the HV electrode's flat surface. The upper and lower rounded electrode edges are covered with an insulative enamel, as shown in Figures 8, 9, and 10.

Figure 11a shows a simulated electric field E in the paper and its vicinity at the HV electrodes side curvature (radius = 3 mm, thickness of the paper is 0.15 mm). The electric field E is somewhat increased in the air as the electrode starts to separate from the paper ($\epsilon_{\mathrm{rAIR}} = 1, \epsilon_{\mathrm{rPAPER}} = 3$). The surface of the paper, which was in the stator slot, is in a region of a uniform electric field E.

Figure 11b shows a simulated electric field E in the paper and its vicinity at the HV electrodes top and bottom curvature, which is covered with an insulating enamel. The increase of electric field E in the air, as the electrode starts to separate from the paper, is smaller than at side curvatures ($\epsilon_{\mathrm{rINSULATIVE\,ENAMEL}} = 3, \epsilon_{\mathrm{rPAPER}} = 3$). Paper top and bottom overhang over the HV electrode edge is about 2 mm. The dimensions and HV electrode edge insulation prevent voltage breakdown through the air, Figure10.

Figure 12 shows an insulation paper sample. The surface of the slot-inserted and extracted paper is annotated with a dotted line rectangle.

In experiments with parameters C and D at low levels (more stress at the stator edge - no or shortest overhang, no cap or a Vitroplast cap only) the paper breakdown puncture occurs most frequently on the line of the stator edge. Imprint

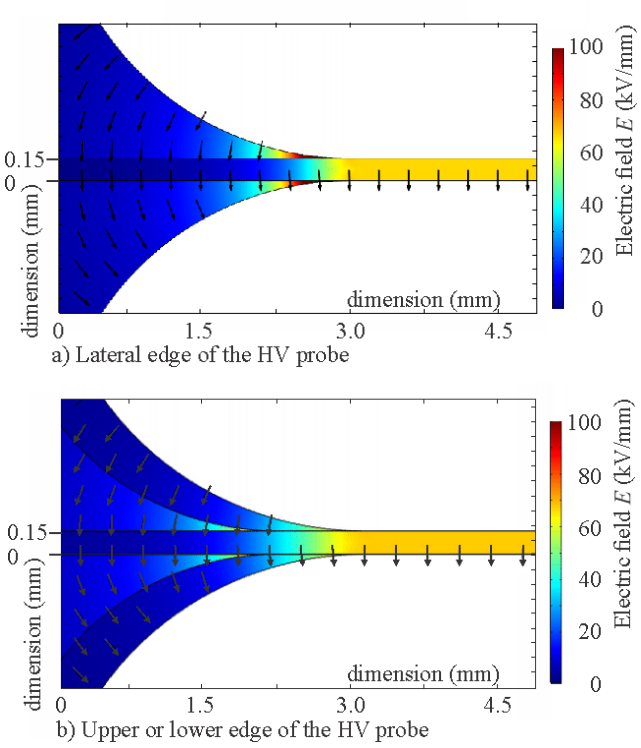

FIGURE 11. The simulated electric field E in the paper and in its vicinity at the HV electrode curvature (radius = 3 mm, paper width = 0.15 mm): a) Lateral edge of the HV electrode, b) Upper or lower edge of the HV electrode.

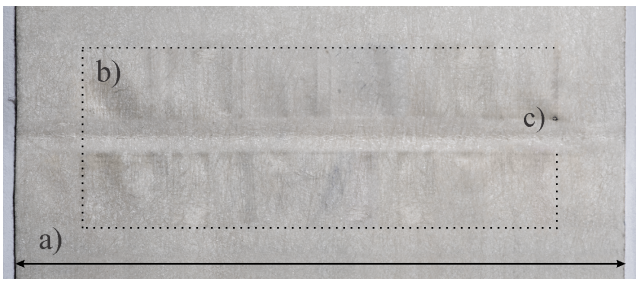

FIGURE 12. A photograph of the insulation paper sample at parameters values A1, B1, C1, and D1: a) Paper width = 71 mm, b) Paper in the slot = 55 mm ∗ 21 mm, c) Pinhole after the breakdown voltage V_B test.

of the stator slot edge is noticeable, as shown in Figure 12, above the c) annotation. The imprint is more intense for a thicker magnet wire (parameter A at a low level).

In experiments with parameters A and B at low levels (thicker wire, less uniform stator slot) and parameters C and D at high levels (less stress at the stator edge) the paper breakdown puncture occurs on the sides of the slot-inserted paper, Figure 12, within the b) annotated rectangle. A pattern of stator blades and their nonuniformities on the slot-inserted paper surface can be observed. Breakdown puncture on the central line (magnet wire pressed to the stator slot bottom) occurs rarely.

Even as the texture of the insulation paper changes and the slot edge gets imprinted after the assembly and disassembly of the complex consisting of the stator slot, insulation paper, and magnet wire, the visual effects do not have enough

TABLE 4. OEM of the parameters *A*, *B*, *C*, and *D* at levels 1...4, Breakdown voltage V_{Bi} , i.e., Result quality η_i at the peak of the Weibull PDF, Means of the breakdown voltageV_{Bi} , i.e., Result quality η_i , and Standard deviations of the Breakdown voltages V_{Bi}, i.e., of Result qualities η_i at 30 repetitions of the same experiment, Weibull distribution parameters α, β, and γ.

i	Parameters A,B,C,D; levels 1...4	V_{Bi}, η_i (V) @ PDF_{PEAK}	Mean V_{Bi}, η_i (V)	V_{Bi}, η_i σ (V), n = 30	α (V)	β	γ (V)
1	1, 1, 1, 1	3433	3362	368	1806	5.1862	1700
2	1, 2, 2, 2	4855	4783	373	1829	5.1839	3100
3	1, 3, 3, 3	6667	6590	333	1824	5.8919	4900
4	1, 4, 4, 4	6356	6294	286	1508	5.6308	4900
5	2, 1, 2, 3	4534	4457	378	1907	5.3540	2700
6	2, 2, 1, 4	4894	4822	332	1754	5.6494	3200
7	2, 3, 4, 1	6385	6313	333	1745	5.5999	4700
8	2, 4, 3, 2	7238	7162	330	1794	5.8516	5500
9	3, 1, 3, 4	6446	6370	316	1797	6.1562	4700
10	3, 2, 4, 3	8240	8172	275	1584	6.2497	6700
11	3, 3, 1, 2	5581	5509	338	1743	5.4976	3900
12	3, 4, 2, 1	5270	5201	298	1621	5.8546	3700
13	4, 1, 4, 2	6185	6121	283	1534	5.8207	4700
14	4, 2, 3, 1	6381	6316	277	1527	5.9343	4900
15	4, 3, 2, 4	8106	8050	246	1348	5.8933	6800
16	4, 4, 1, 3	7821	7755	287	1570	5.8780	6300

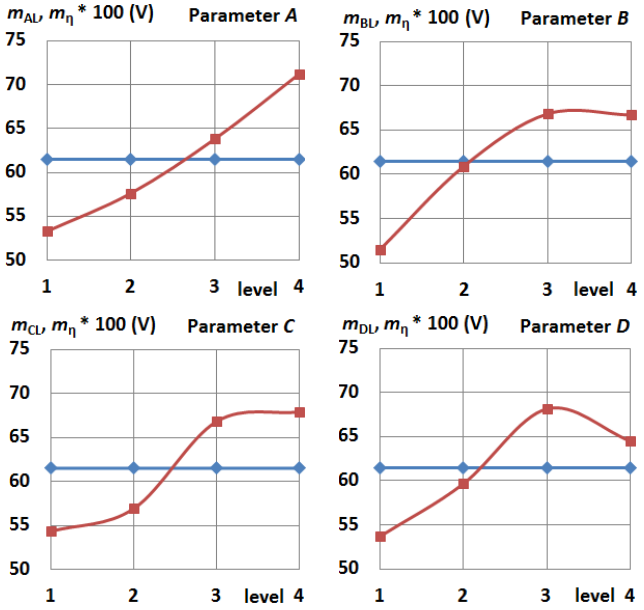

FIGURE 13. Means m_{PL} of result qualities η_i – red rectangles, and mean m_η of result qualities η_i – blue diamonds.

significant differences at different parameter levels to be directly used as the quality function η. Plane visual damage assessment would rely heavily on a subjective component. The S/N ratio would be just too low if using plane visual damage assessment as a measure of result quality η. We did not study paper damage with magnification and image analysis tools.

Voltage breakdown creates a pinhole through the paper with a small burn around it, Figure 12, annotation c). In the IEC 60243-1 proposed setup, which we follow as much as possible, the occurrence of the first hole shuts down the voltage. According to the parameters level, the pinhole occurs in the expected area.

C. INDUCED DATA

The mean value m_η of all 16 result qualities η_i (the 3rd column of the Table 4 - η_i at the PDF peak value) is calculated by (1); the mean values of 4 result qualities η_i for experiments with parameter P at level L m_{PL} are calculated by (2):

$$\begin{aligned} m_\eta &= 6149 \\ m_{A1} &= 5328,\ m_{A2} = 5763,\ m_{A3} = 6384,\ m_{A4} = 7123, \\ m_{B1} &= 5149,\ m_{B2} = 6092,\ m_{B3} = 6685,\ m_{B4} = 6671, \\ m_{C1} &= 5432,\ m_{C2} = 5691,\ m_{C3} = 6683,\ m_{C4} = 6791, \\ m_{D1} &= 5367,\ m_{D2} = 5965,\ m_{D3} = 6815,\ m_{D4} = 6450. \end{aligned}$$

m_{PL} and m_η are displayed in Figure 13.

For the data in the 3rd column of the Table 4, one calculates the total sum of squares SS_T from (14), the sum of squares of the parameters SS_A, SS_B, SS_C, and SS_D from (15) and the sum of squares of error SS_{ERR} from (19).

$$SS_T = 27023436,\quad SS_A = 1828145,\quad SS_B = 1561965,$$
$$SS_C = 1421227,\quad SS_D = 1180205,\quad SS_{ERR} = 764317.$$

Corresponding variance ratios expressed in the sums of squares (14), (15), are as follows:

$$4\,SS_A/SS_T = 0.27,\ 4SS_B/SS_T = 0.23,\ 4SS_C/SS_T = 0.21,$$
$$4\,SS_D/SS_T = 0.17,\quad 4SS_{ERR}/SS_T = 0.11.$$

These ratios are presented in Figure 14 on the left.

Fisher factors for data in the OEM are calculated by (21): $FF_A = 2.39$, $FF_B = 2.04$, $FF_C = 1.86$, $FF_D = 1.54$. These are shown in Figure 14 right.

Fisher factors are small. The 95 % confidence interval (26) is ±1010 V. Interparameter influence needs to be incorporated into the calculation. We add the virtual parameter E to the analysis to incorporate the interparameter influence on η (Table 3). By (2),

$$m_{E1} = 6754,\quad m_{E2} = 6377,\quad m_{E3} = 5754,\quad m_{E4} = 5713.$$

By (15), $SS_E = 764317$. By (19), modified for SS_E inclusion, is $SS_{ERR} = 0$.

Ratios of sums of squares, m_{EL} and m_η are displayed in Figure 15.

By (25),

$$\begin{aligned} \eta_{MAX} = V_{BMAX} &= m_\eta \\ &+ (m_{A4} - m_\eta) + (m_{B3} - m_\eta) \\ &+ (m_{C4} - m_\eta) + (m_{D3} - m_\eta) + (m_{E1} - m_\eta) \\ &= 6149 + (7123 - 6149) + (6685 - 6149) \\ &+ (6791 - 6149) + (6815 - 6149) \\ &+ (6754 - 6149) = 9572\text{V}. \end{aligned} \tag{27}$$

In (27), the virtual parameter E is at level 1. The rationale is that, at η_{MAX}, the least parameter interactions should take place due to the physical nature of this experiment. Picking

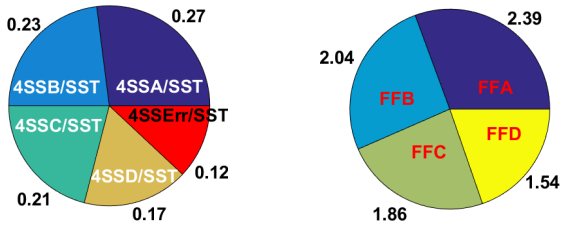

FIGURE 14. Ratios of sums of squares - left, Fisher factors – right.

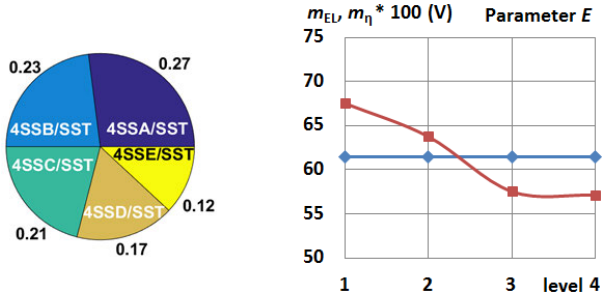

FIGURE 15. Ratios of sums of squares - left; means m_{EL} of result qualities η_i – red rectangles, and mean m_η of result qualities η_i – blue diamonds - right.

the most suitable virtual parameter E level L in a certain experiment is the experimenter's choice. Other viable calculated η_{MAX} values are 9194 V, 8571 V, and 8530 V for virtual parameter E at levels 2, 3, and 4. For any of the 4 E parameter levels the confidence interval equals 0, since SS_{ERR} equals 0.

By (25), η for best performance – thickest magnet wire ($A1$), highest slot smoothness ($B4$), shortest overhang ($C1$), and Nomex spacer ($D3$) is calculated by (28):

$$\begin{aligned}\eta_{BEST\_PERF} &= V_{BBEST\_PERF} = m_\eta + (m_{A1} - m_\eta) \\ &\quad + (m_{B1} - m_\eta) + (m_{C1} - m_\eta) \\ &\quad + (m_{D3} - m_\eta) + (m_{E3} - m_\eta) \\ &= 6149 + (5328 - 6149) + (6671 - 6149) \\ &\quad + (5432 - 6149) + (6815 - 6149) \\ &\quad + (5754 - 6149) = 5404\ V \end{aligned} \tag{28}$$

In (28), we picked the virtual parameter E at level 3 since best performance parameters put a complex mechanical load on paper insulation. Other viable calculated η_{BEST_PERF} values are 6404 V, 6027 V, and 5363 V for the virtual parameter E at levels 1, 2, and 4. Confidence interval is 0.

Some 17 % increase in torque (derived from the data in the section on Problem formulation) causes production-induced insulation paper damage and decreases the calculated insulation paper breakdown voltage for 43 %. Such a performance motor passes all production tests but this calculation and previous practical experience show that an early failure will take place.

V. THE CONTROL EXPERIMENT

The calculated optimal i.e., maximum insulation paper breakdown voltage V_{BOPT} is 8967 V by (24) with an error Err

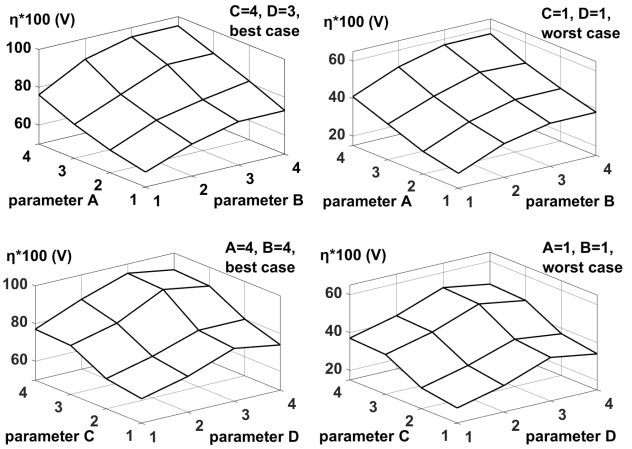

FIGURE 16. Result quality η vs. levels of physical parameters.

value of 0 V. The error is reflected in the ±1010 V of the 95 % confidence interval, by (26). V_{BOPT} is 9572 V by (25) without ambiguity. The corresponding confidence interval is 0 V (SS_{ERR} equals 0). The best parameters level is identified as:

a) Thinnest magnet wire, w = 2.20 mm,
b) Stator slot smoothness better than 0.1 mm,
c) Straight length of the magnet wire after the slot exit is 2.10 mm,
d) Nomex insulation cap.

30 repetitions of the control experiment with the best parameters level result in the breakdown voltage $V_B = 9560$ V with a 95 % confidence interval $2\sigma = \pm 530$ V, which results in the 95 % confidence interval between 9560 V - 589 V and 9560 V + 471 V (Weibull distribution: V_B at PDF_{MAX} = 9560 V, V_{Bmean} = 9501 V, σ = 265 V). The calculated result (27) is just on the spot of the control experiment measurement. It is also important that 30 repetitions of measuring V_B on an intact insulation paper yield V_B = 9595 V with the 95 % confidence interval between 9595 V - 728 V and 9595 V + 572 V (Weibull distribution: V_B at $PDF_{MAX} = 9595$ V, $V_{Bmean} = 9516$ V, $\sigma = 325$ V).

VI. RESULTS

Figure 16 shows result quality η vs. levels of physical parameters. η is calculated by (25) where the parameters level L_{BEST} is changed to the parameters level needed in formation of the meshes. Virtual parameter E level, which models inter-parameter influence on η, is incorporated in (25) the same as the physical parameters level. It is our understanding that in combinations of physical parameter levels that result in less insulation paper damage, where the complexity of the damage process is lower, E levels 1 and 2 (Figure 15) are appropriate contributors. Intense damage can be correlated with more interactions among parameter influences; corresponding E levels are 3 and 4. An educated, but somewhat subjective choice of the E level at each combination of physical parameters in the calculation of η is not desirable; the alternative is

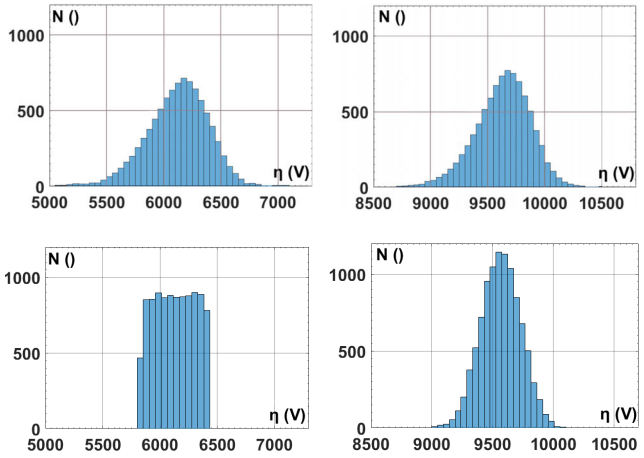

FIGURE 17. Mapping of input data distributions into best result η distributions.

having a 95 % confidence interval (26) of ±1010 V, which is a much poorer option. Inclusion of the virtual parameter E for modeling cross-factor effects results in a firm result value with a confidence interval of 0 V.

Grids in Figure 16 show some interparameter influence on the result quality η, as seen also in terms of $4SS_P/SS_T$ ratios in Figures 14 and 15.

The last remaining issue is a mapping of the 16 measured η_i confidence levels, actually variances σ_i^2 into the variance σ^2 of the calculated best result η_{BEST}. Effects of the 16 result quality variances σ^2, resulting from the 30 experiment repetitions, need consideration at all derived results. We solve this problem by running an experiment in our custom-built simulator of equations.

First, we simulate the distributions of the 16 η_i. Figure 17, top left shows one of the 16 η_i distributions, namely the η_{13} distribution. Figure 17, top right shows the distribution of the η_{MAX}. After 10000 iterations, the η_{MAX} at peak of simulation produced PDF is 9696 V, which is 1.3 % above the η_{MAX}, calculated from the 16 η_i in (27).

Then, we simulate rectangular input distributions. Figure 17, bottom left, shows the η_{13} rectangular distribution with boundaries at 5821 V and 6421 V (Table 4, column 4: 6121 V, ±300 V). The η_{MAX} distribution is at the right in Figure 17. After 10000 iterations, the $\eta_{MAXmean}$ is at 9567 V, which is 0.6 % above the η_{MAX} which would be calculated by (25) from the 16 V_{Bi} mean values (Table 4, column 4). σ of the simulated η_{MAX} is 163 V. The results after even more iterations are the same.

Figure 18 shows histograms of the best parameters level in Figure 17's simulation. Observation of not-single selection of B and C levels can be disappointing at first glance. Clarification is achieved by observation of Figure 19 data in real-time fluctuations, caused by simulation with scattered inputs η_i. We made 2 short movies of the fluctuations for possible download and display, Reference [63]. Input data of each of the 16 measured η_i have a rectangular distribution, the same as for production of the results in Figures 17 and 18.

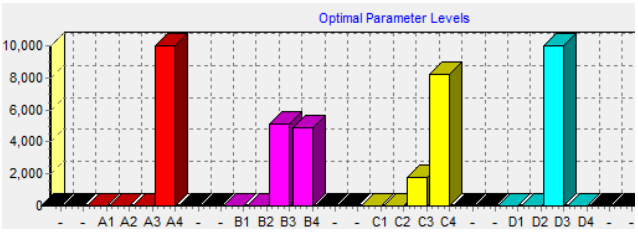

FIGURE 18. The best result parameters level, for a uniform/rectangular distribution of measured data.

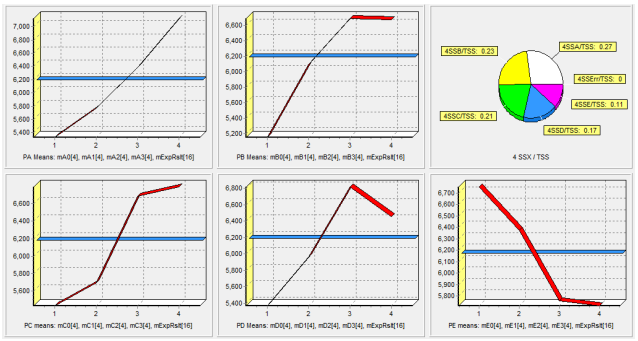

FIGURE 19. m_η, m_{AL}, m_{BL}, m_{CL}, m_{DL}, m_{EL} and ratios of 4 SS_P / SS_T in the simulator window.

Figure 19 presents m_η, m_{AL}, m_{BL}, m_{CL}, m_{DL}, m_{EL} at all 4 levels and $4SS_P/SS_T$ ratios (the same information as in Figures 13 and 15, but as a simulator print-screen). SS_{ERR} equals 0 in all calculation iterations, m_η, m_{AL}, m_{BL}, m_{CL}, m_{DL}, and m_{EL} and ratios of $4SS_P/SS_T$ vibrate according to variations of the 16 input data η_i.

The means m_{B3} and m_{B4}, Figures 13 and 19, have the most similar values. A slight change in values of the 16 measured results η_i changes the slope of the B curve between levels 3 and 4, mid top in Figure 19. This results in $B3$ $B4$ uncertainty. $C3$ $C4$ uncertainty, Figure 19 bottom left, is produced by the same principle. Based on its slope the $C3$ $C4$ uncertainty is less sensitive to input data fluctuations.

Observation of Figures 18 and 19 yields $A4$, $B4$, $C4$, and $D3$ as the optimum parameters level. $B3$ can be an alternative to $B4$ in the stator cost optimization process. $C4$ is the most dependable choice – in close to 2500 out of 10000 simulations $C3$ suffices.

Confidence in the results of the experiments comes from the relatively small scattering of the 30 measurements of each of the 16 experiments, per Table 4. The influence of experimental parameters is significantly above the influence of noise parameters (as are the rate and the pressure for magnet wire insertion).

VII. DISCUSSION

A. INSULATION DAMAGE MECHANISM

The physical mechanism of insulation paper damage in the assembly phase of the motor is a modification of the synthetic layer paper structure caused by excessive local high pressure peaks. Local pressure peaks appear on square slot edges and on edges between the less than perfectly produced and

aligned blades of the stator bladepack. Paper manufacturers provide data on tensile strength, but not on the tolerable peaks of lateral pressure in static (assembled complex) and dynamic environment (assemblage of the complex).

The physical mechanism of insulation paper damage and the consequential further reduction of the breakdown voltage V_B in the exploitation phase of the motor are related to the transfer of energy in different forms between magnet wire and stator slot through the assembly-weakened insulation paper. Electro, and magneto dynamic, and elevated temperature induced forces are affecting the initial damage at elevated temperature over time. At some stage of damage development the inception of partial discharges takes over the deterioration process. Partial discharges intensify the damage process and bring it to a point of insulation breakdown in a short time [54]. The literature does not report on the mechanisms of damage development in a mechanically pre-damaged insulation paper.

B. CHOICE OF THE RESULT QUALITY η VARIABLE

The choice of a variable that is mapped to the experiment quality η is most important in the creation of designed experiments. The variable needs to be well responsive to the levels of the parameters. The accuracy of the η value measurement is far less important than the repeatability and strong coupling between the parameters level and the η value.

Let us justify this claim in a few steps.

a) A potential measurement error affects all measurements.

b) An optimal result η_{OPT} and the optimal parameters level are calculated from error affected measurements.

c) A potential measurement error affects the measured optimal result quality η.

d) The calculated and the measured optimal result quality η_{OPT} are compared. Comparison of the two η values practically nullifies the error influence on each of them. The potential difference between the calculated and the measured optimal result η_{OPT} is not much different from the case without an error.

In our experiments we are able to calculate the parameters level that produces no detectable insulation paper damage. The calculated best parameters level is challenged by a physical control experiment. The breakdown voltage at the optimal parameters level is statistically equal to the breakdown voltage of an intact insulation paper. However, such a favorable optimization outcome is not guaranteed for any designed experiment at all. The calculated and experimentally confirmed optimal result can still be nonoptimal from the point of view of the experimenter's requirements and expectations. This discrepancy cannot be solved mathematically. In such situations additional parameter levels have to be introduced and their influence on the result quality η evaluated. If this is insufficient, a deeper insight into the problem is needed, and the experiment set-up must be adjusted with the help of additional knowledge.

The new procedure for finding the optimal parameters level in the presence of inter-parameter influences on the result quality η, presented in this paper, just always calculates the optimum result without uncertainty range. The optimum target can be defined as minimum or maximum, or any value in-between – the choice depends on the nature of the experiment. Whether the optimal η is good enough and how to proceed if it is not, is left to the experimenters' judgment.

The question remains regarding whether the AC breakdown voltage is an optimal choice for the assessment of the insulation paper damage. The IEC 60243-1 standard on AC testing electric strength of insulating materials states that the test results obtained in accordance with the standard are useful for detecting deviations from the normal material characteristics. The deviations can result from processing variables, manufacturing situations and other factors. Yet, we cannot follow the standard completely because our electrodes dimensions are governed by the stator slot dimensions. Our measurement probably does have some offset, compared to a strict standard measurement. As already explained, the error is not desired, but it is not a crucial factor in finding the optimal parameters level. This is the beauty of ratiometric measurements, compared to absolute ones. Measurement repeatability is important and this we have.

Technically, other types of voltage measurements are far more in line with the constraints of a PWM voltage driven motor than simple to conduct AC HV test. A repetitive HV square wave signal at some typical PWM frequency could fit better to the in-wheel motor drive constraints. References [64], [65] report construction of an HV generator that creates square wave signal at 10 kHz, $V_{PPMAX} = 8$ kV, with signal rise and fall times of more than 20 ns. This generator is used for insulation endurance tests. Square wave generators with large voltage amplitude and short transition times are not widely available due to technical constraints. The next issue could be matching of test apparatus voltage transition times with those of a particular motor inverter. Preservation of voltage transition times while ramping up the voltage would be most challenging in a PWM breakdown test, structured same as the AC HV breakdown test.

A PDIV measurement could give a good insight into the paper damage level. Reference [66] measures the PDIV for resin. The ratios of PDIVs measured at specimen being in an inert liquid and in an open air are between 7 and 4, depending on resin cavities size. The presence of air would decrease S/N ratio in our experimental work. Special setups would prolong experimenting time.

Regarding the fitness of the AC HV test for assessing the paper insulation damage we also consulted our technical partner – a producer of synthetic layered insulation papers. In the paper insulation industry AC HV tests are performed by the IEC 60243-1, PDIV test is performed by the ASTM 1868, 3 AC tests at different voltages are performed for endurance evaluation, and a pulse endurance test with bipolar square wave at values 1500, 0, and -1500 V is performed at 180° C. The illustrative values for a 0.15 mm thick NMN paper are: AC $V_B = 9$ kV, PDIV $= 1$ kV, and a non-ambitious pulse endurance test is at 50 hours. Increase of pulse endurance

is a matter of current developments and is under a nondisclosure agreement. The PWM breakdown voltage has to be lower than the AC breakdown voltage – a PWM frequency is typically 300 times higher than the IEC 60342-1 frequency, and a typical 50 ns transition time is 400 000 times shorter than a 50 Hz period. The electrical stress on the insulation at a certain voltage level is enormously higher at a PWM test than at an AC test.

C. TOLERANCES AND MATERIALS DETAIL

The dimensional tolerances of the materials, we used in the study are available in the file ''Tolerances.pdf'', in [63].

The measured data and fitted distributions are available in the file ''Distributions.pdf'', in [63].

We cannot use any greasing substance in order to insert the paper and/or winding into the slot because grease or lube would decrease friction between magnet wire and insulation paper in the assembly and in the exploitation phase. Less friction in the latter works against rigidity of the stator complex. Grease or lube could have negative influence on adhesion between epoxy resin and the assembled complex. Grease or lube would not decrease excessive local high pressure peaks that appear on square slot edges and on edges between the less than perfectly produced and aligned blades of the stator bladepack.

We cannot use hot-formed insulating paper. Our slots are of same width from bottom to top, Figure 3. We insert the insulation paper in the form of a continuous stripe, Figure 6. We cut the paper at slot tops after magnet wire insertion. Hot-formed paper edges at slot side ends would not bring any benefit to our insulation system since they would have to appear on the outer side of the insulation cap.

We cannot use a rectangular magnet wire, which would maximize slot fill factor. The shortest magnet wire overhang contributes to the fulfillment of the high torque requirement in our patented design of a compact multiphase wave winding [67]. The use of rectangular magnet wire would require wire bending in the short overhangs. Currently we have to stay with the round magnet wire.

The use of materials on the high limit of the tolerances in the IEC dimensional standards yields $A4$, $B4$, $C4$, and $D3$ as the optimum parameters level. Best result quality η_{MAX}, i.e., V_{BMAX} still reaches breakdown voltage V_B of the intact paper.

D. OEM AND INTER-PARAMETER INFLUENCE ON THE RESULT QUALITY η

The designed experiments are structured into the OEM to establish optimal parameters level at a manageable amount of experimental work.

Structuring designed experiments on the basis of orthogonality implies that we expect the additive model to be suited to the nature of the experiment. The discrepancy between the additive model and the nature of the physical experiment is exhibited in the size of SS_{ERR} (19). The confidence interval i.e., section of ambiguity regarding the result value is derived from SS_{ERR}. The size of Fisher factors, derived with the help of SS_{ERR}, is a measure of conformity between the model and the physical experiment. One hopes for small SS_{ERR} (high Fisher factors). Were that not the case, the physical experiment would need restructuring. The aim is to have a better experiment fitting to the capabilities of the analysis. Experiment restructuring brings new unknowns.

Inclusion of virtual parameter(s) extends the additive modeling to experiments with interparameter effects. In this study, inclusion of one 4-level virtual parameter suffices for satisfactory analysis. The only remaining question is which level of the virtual parameter to add to the combination of physical parameters in each calculation of result η. The nature of the physical experiment suggests choices.

Our experience is that the time put into numerical exploration and verification of concepts is well invested. Building up a numerical analysis tool is an interactive learning process. Running cases adds confidence to analysis build-up and to results.

Orthogonality in the OEM is achieved and exploited as follows: Each level of each parameter appears in experiments where all other parameters rank through all their levels. When so, contributions of each level of each parameter can be calculated as the means of those experiments where they appear. Such balancing of values into means gives correct results as long as the influence of any level of any parameter is not correlated with any level of any other parameter. As soon as such a correlation occurs, the environment properties are no longer the same in experiments with parameter P at levels 1, 2, 3, and 4.

Parameter cross-correlation annihilates OEM orthogonality – consequentially cross-correlation annihilates the validity of additive modeling. Addition of (enough) virtual parameter(s) can result in additivity of physical and virtual parameter effects on the result quality η. A short video on this project is available in [63].

An alternative to this approach is relying on the use of commercial modeling tools. It is however safer from the product development view, and more rewarding, to develop particular product and production-critical knowledge from basics than to rely on other's expertise in the area of common problem solutions.

VIII. CONCLUSION

Results of this research enable faster definition of the optimal values for the thickness of the magnet wire and smoothness of the slot, the length of the straight magnet wire at the slot end and the type of insulation cap. The contributions are:

a) Dimensions and materials of the complex are selected: stiff magnet wire and insulation paper in the slot, stator slot smoothness, straight magnet wire between the end of the slot and the start of the magnet wire curvature, and insulation cap at the slot end. The selection criterion is preservation of the paper insulation strength in the tight assembly of the complex.

b) Interdependent influence of dimensional parameters and material on the paper insulation deterioration in the studied tight assembly is identified.

c) Material and dimensional parameters are ranked by their influence on deterioration of the insulation paper in the tight assembly.

d) Sensitivity of the insulation paper deterioration to the dimensional parameters and to the material in the tight assembly is identified.

e) A formal procedure is devised for ranking dimensional and material parameters of the assembly as either interdependent or independent, based on their influence on potential deterioration of the insulation paper properties.

f) Formal procedures are devised for the prediction of the insulation paper deterioration level when parameters have independent or interdependent influence on the deterioration. The best prediction (unharmed insulation paper) is verified by the control experiment.

The demonstrated approach can be adapted to other problems with independent or interdependent parameter influences on the result quality η. The problems can have a different number of parameters with a different number of levels and different formulation of result quality η. Simulation of equations is advised in verification of potential adaptations.

ACKNOWLEDGMENT

M. Jenko thanks to Prof. E. Grgin, ret. from Yeshiva University and Boston University; Prof. J. Zerovnik at University of Ljubljana, M.Sc. A. Detela at Elaphe Ltd., Ljubljana, and J. Hildenbrand, dipl. ing. (FH) at Krempel Group, Vaihingen for their discussions.

REFERENCES

[1] C. Lin and Z. Xu, "Wheel torque distribution of four-wheel-drive electric vehicles based on multi-objective optimization," *Energies*, vol. 8, no. 5, pp. 3815–3831, Apr. 2015. Accessed: Jul. 31, 2019, doi: 10.3390/en8053815.

[2] L. Zhai, T. Sun, and J. Wang, "Electronic stability control based on motor driving and braking torque distribution for a four in-wheel motor drive electric vehicle," *IEEE Trans. Veh. Technol.*, vol. 65, no. 6, pp. 4726–4739, Jun. 2016, doi: 10.1109/tvt.2016.2526663.

[3] R. Hou, L. Zhai, and T. Sun, "Steering stability control for a four hub-motor independent-drive electric vehicle with varying adhesion coefficient," *Energies*, vol. 11, no. 9, p. 2438, Sep. 2018. Accessed: Jul. 31, 2019, doi: 10.3390/en11092438.

[4] R. Hou, L. Zhai, T. Sun, Y. Hou, and G. Hu, "Steering stability control of a four in-wheel motor drive electric vehicle on a road with varying adhesion coefficient," *IEEE Access*, vol. 7, pp. 32617–32627, 2019. Accessed: Jul. 31, 2019, doi: 10.1109/access.2019.2901058.

[5] X. Shao, F. Naghdy, H. Du, and Y. Qin, "Coupling effect between road excitation and an in-wheel switched reluctance motor on vehicle ride comfort and active suspension control," *J. Sound Vibrat.*, vol. 443, pp. 683–702, Mar. 2019, doi: 10.1016/j.jsv.2018.12.012.

[6] S. Nie, Y. Zhuang, F. Chen, Y. Wang, and S. Liu, "A method to eliminate unsprung adverse effect of in-wheel motor-driven vehicles," *J. Low Freq. Noise, Vibrat. Act. Control*, vol. 37, no. 4, pp. 955–976, Dec. 2018, doi: 10.1177/1461348418767096.

[7] F. Yang, L. Zhao, Y. Yu, and C. Zhou, "Analytical description of ride comfort and optimal damping of cushion-suspension for wheel-drive electric vehicles," *Int. J. Automot. Technol.*, vol. 18, no. 6, pp. 1121–1129, Dec. 2017, doi: 10.1007/s12239-017-0109-2.

[8] A. Łebkowski, "Design, analysis of the location and materials of neodymium magnets on the torque and power of in-wheel external rotor PMSM for electric vehicles," *Energies*, vol. 11, no. 9, p. 2293, Aug. 2018. Accessed: Jul. 31, 2019, doi: 10.3390/en11092293.

[9] G. Hong, T. Wei, and X. Ding, "Multi-objective optimal design of permanent magnet synchronous motor for high efficiency and high dynamic performance," *IEEE Access*, vol. 6, pp. 23568–23581, 2018. Accessed: Jul. 31, 2019, doi: 10.1109/access.2018.2828802.

[10] G. Gotovac, A. Detela, G. Lampič, and J. Valentinčič, "Analytical and FEM approach to reduce the cogging torque in in-wheel motors," *Elect. Eng.*, vol. 97, no. 4, pp. 269–275, Dec. 2015, doi: 10.1007/s00202-015-0334-5.

[11] T. Ishigami, Y. Tanaka, and H. Homma, "Development of motor stator with rectangular-wire lap winding and an automatic process for its production," *Elect. Eng. Jpn.*, vol. 187, no. 4, pp. 51–59, Jun. 2014, doi: 10.1002/eej.22522.

[12] H. Saavedra, J.-R. Riba, and L. Romeral, "Multi-objective optimal design of a five-phase fault-tolerant axial flux PM motor," *Adv. Elect. Comput. Eng.*, vol. 15, no. 1, pp. 69–76, 2015, doi: 10.4316/aece.2015.01010.

[13] Y. B. Deshpande, H. A. Toliyat, S. S. Nair, S. J. Dhinagar, S. Immadisetty, and S. Nalakath, "High-torque-density single tooth-wound bar conductor permanent-magnet motor for electric two wheeler application," *IEEE Trans. Ind. Appl.*, vol. 51, no. 3, pp. 2123–2135, May 2015, doi: 10.1109/tia.2014.2369822.

[14] G. Zhang, W. Hua, M. Tong, and M. Cheng, "Design and manufacturing considerations of flux-switching permanent magnet motors for mass productions used in EVs and HEVs," presented at the 18th Int. Conf. Elect. Mach. Syst. (ICEMS), 2016, pp. 1757–1763, doi: 10.1109/ICEMS.2015.7385325.

[15] P. Stenzel, "Needle winding for distributed round-wire-windings without the use of insulation disks," presented at the 4th Int. Electr. Drives Prod. Conf. (EDPC), 2014, doi: 10.1109/EDPC.2014.6984387.

[16] B. Jokanović, M. Bebić, and N. Kartalović, "The influence of combined strain and constructive solutions for stator insulation of rotating electrical machines on duration of their reliable exploitation," *Int. J. Electr. Power Energy Syst.*, vol. 110, pp. 36–47, Sep. 2019, doi: 10.1016/j.ijepes.2019.02.041.

[17] N. Lahoud, M. Q. Nguyen, P. Maussion, D. Malec, and D. Mary, "Lifetime model of the inverter-fed motors secondary insulation by using a design of experiments," *IEEE Trans. Dielectr. Electr. Insul.*, vol. 22, no. 6, pp. 3170–3176, Dec. 2015, doi: 10.1109/tdei.2015.005202.

[18] T. G. Arora and M. V. Aware, "Life model for PWM controlled induction motor insulation using design of experiments method," *Electr. Power Compon. Syst.*, vol. 47, nos. 1–2, pp. 153–163, Jan. 2019, doi: 10.1080/15325008.2019.1566843.

[19] V. Iosif, D. Roger, S. Duchesne, and D. Malec, "Assessment and improvements of inorganic insulation for high temperature low voltage motors," *IEEE Trans. Dielectr. Electr. Insul.*, vol. 23, no. 5, pp. 2534–2542, Oct. 2016, doi: 10.1109/tdei.2016.7736810.

[20] X. Qiao, Z. Zhang, X. Jiang, X. Li, and Y. He, "A new evaluation method of aging properties for silicon rubber material based on microscopic images," *IEEE Access*, vol. 7, pp. 15162–15169, 2019. Accessed: Jul. 31, 2019, doi: 10.1109/access.2019.2892143.

[21] M. Riera-Guasp, J. A. Antonino-Daviu, and G.-A. Capolino, "Advances in electrical machine, power electronic, and drive condition monitoring and fault detection: State of the art," *IEEE Trans. Ind. Electron.*, vol. 62, no. 3, pp. 1746–1759, Mar. 2015, doi: 10.1109/tie.2014.2375853.

[22] G.-A. Capolino, J. A. Antonino-Daviu, and M. Riera-Guasp, "Modern diagnostics techniques for electrical machines, power electronics, and drives," *IEEE Trans. Ind. Electron.*, vol. 62, no. 3, pp. 1738–1745, Mar. 2015, doi: 10.1109/tie.2015.2391186.

[23] F. Duan and R. Zivanovic, "Condition monitoring of an induction motor stator windings via global optimization based on the hyperbolic cross points," *IEEE Trans. Ind. Electron.*, vol. 62, no. 3, pp. 1826–1834, Mar. 2015, doi: 10.1109/tie.2014.2341563.

[24] F. R. Blanquez, M. Aranda, E. Rebollo, F. Blazquez, and C. A. Platero, "New fault-resistance estimation algorithm for rotor-winding ground-fault online location in synchronous machines with static excitation," *IEEE Trans. Ind. Electron.*, vol. 62, no. 3, pp. 1901–1911, Mar. 2015, doi: 10.1109/tie.2014.2336612.

[25] W. Mcdermid and T. Black, "Strategies to maximize life of rotating machines windings," *IEEE Trans. Dielectr. Electr. Insul.*, vol. 22, no. 6, pp. 3087–3098, Dec. 2015, doi: 10.1109/tdei.2015.005179.

[26] F. Salameh, A. Picot, M. Chabert, and P. Maussion, "Parametric and nonparametric models for lifespan modeling of insulation systems in electrical machines," *IEEE Trans. Ind. Appl.*, vol. 53, no. 3, pp. 3119–3128, May 2017, doi: 10.1109/tia.2016.2635100.

[27] F. Salameh, "Variable importance assessment in lifespan models of insulation materials: A comparative study," presented at the SDEMPED, IEEE 10th Int. Symp. Diagnostics Elect. Mach., Power Electron. Drives, 2015, pp. 198–204, doi: 10.1109/DEMPED.2015.7303690.

[28] F. Salameh, A. Picot, M. Chabert, and P. Maussion, "Regression methods for improved lifespan modeling of low voltage machine insulation," *Math. Comput. Simul.*, vol. 131, pp. 200–216, Jan. 2017, doi: 10.1016/j.matcom.2015.11.001.

[29] P. Maussion, "Lifespan and aging modeling methods for insulation systems in electrical machines: A survey," presented at the IEEE Workshop Elect. Mach. Design, Control Diagnosis (WEMDCD), 2015, pp. 279–288, doi: 10.1109/WEMDCD.2015.7194541.

[30] S. Lee, S. Cho, K. Kim, J. Jang, T. Lee, and J. Hong, "Optimal design of interior permanent magnet synchronous motor considering the manufacturing tolerances using Taguchi robust design," *IET Electr. Power Appl.*, vol. 8, no. 1, pp. 23–28, Jan. 2014, doi: 10.1049/iet-epa.2013.0109.

[31] G. Lei, J. G. Zhu, Y. G. Guo, J. F. Hu, W. Xu, and K. R. Shao, "Robust design optimization of PM-SMC motors for six sigma quality manufacturing," *IEEE Trans. Magn.*, vol. 49, no. 7, pp. 3953–3956, Jul. 2013, doi: 10.1109/tmag.2013.2243123.

[32] G. Lei, T. Wang, J. Zhu, Y. Guo, and S. Wang, "System-level design optimization method for electrical drive systems–robust approach," *IEEE Trans. Ind. Electron.*, vol. 62, no. 8, pp. 4702–4713, Aug. 2015, doi: 10.1109/tie.2015.2404305.

[33] Z. Xiang, X. Zhu, L. Quan, Y. Du, C. Zhang, and D. Fan, "Multilevel design optimization and operation of a brushless double mechanical port flux-switching permanent-magnet motor," *IEEE Trans. Ind. Electron.*, vol. 63, no. 10, pp. 6042–6054, Oct. 2016, doi: 10.1109/tie.2016.2571268.

[34] P. Chrin, "Improvements on experimental modeling of the losses in induction machine with Taguchi orthogonal plan," presented at the IECON, 41st Annu. Conf. IEEE Ind. Electron. Soc., 2015, pp. 4836–4841, doi: 10.1109/IECON.2015.7392857.

[35] M. Vukotić and D. Miljavec, "Design of a permanent-magnet flux-modulated machine with a high torque density and high power factor," *IET Electr. Power Appl.*, vol. 10, no. 1, pp. 36–44, Jan. 2016, doi: 10.1049/iet-epa.2015.0143.

[36] A. Sorgdrager, R.-J. Wang, and A. Grobler, "Taguchi method in electrical machine design," *SAIEE Afr. Res. J.*, vol. 108, no. 4, pp. 150–164, Dec. 2017, doi: 10.23919/saiee.2017.8531928.

[37] J.-T. Tsai, C.-C. Chang, W.-P. Chen, and J.-H. Chou, "Optimal parameter design for IC wire bonding process by using fuzzy logic and Taguchi method," *IEEE Access*, vol. 4, pp. 3034–3045, 2016. Accessed: Jul. 31, 2019, doi: 10.1109/access.2016.2581258.

[38] A. A. Md Ralib and A. N. Nordin, "Application of Taguchi signal to noise ratio design method to ZnO thin film CMOS SAW resonators," *IEEE Access*, vol. 7, pp. 27993–28000, 2019. Accessed: Jul. 31, 2019, doi: 10.1109/access.2019.2900590.

[39] S. M. L. M. C. Kulan, N. J. Baker, J. D. Widmer, "Modelling the mechanical and thermal properties of compressed stator windings," presented at the 8th IET Int. Conf. Power Electron., Mach. Drives (PEMD), Apr-2016, pp. 1–6, doi: 10.1049/CP.2016.0132.

[40] *Uniform Provisions Concerning the Approval of Vehicles With Regard to Specific Requirements for the Electric Power Train*, United Nations, United Nations Econ. Commission Eur., Geneva, Switzerland, 2013.

[41] *Insulation Coordination for Equipment Within Low-Voltage Systems—Part 1: Principles, Requirements and Tests*, Standard 60664-1, IEC, 2007.

[42] *Electrically Propelled Road Vehicles, Safety Specifications, Protection of Persons Against Electric Shock*, Standard 6469-3, ISO, 2011.

[43] P. Wang, A. Cavallini, and G. C. Montanari, "Characteristics of PD under square wave voltages and their influence on motor insulation endurance," *IEEE Trans. Dielectr. Electr. Insul.*, vol. 22, no. 6, pp. 3079–3086, Dec. 2015, doi: 10.1109/tdei.2015.005158.

[44] G. C. Montanari and F. Ciani, "Inverter design and partial discharge phenomenology in insulation systems of rotating machines," presented at the IEEE Int. Electr. Mach. Drives Conf. (IEMDC), 2017, doi: 10.1109/IEMDC.2017.8001863.

[45] G. C. Stone and G. H. Miller, "Progress in rotating-machine insulation systems and processing," *IEEE Electr. Insul. Mag.*, vol. 29, no. 4, pp. 45–51, 2013, doi: 10.1109/MEI.2013.6545259.

[46] A. Contin, M. Piller, and G. Schena, "Analysis of 3D computed tomographic imaging of ground-wall insulation for AC rotating machines," *IEEE Trans. Dielectr. Electr. Insul.*, vol. 22, no. 3, pp. 1520–1529, Jun. 2015, doi: 10.1109/tdei.2015.7116347.

[47] N. Lahoud, J. Faucher, D. Malec, and P. Maussion, "Electrical aging of the insulation of low-voltage machines: Model definition and test with the design of experiments," *IEEE Trans. Ind. Electron.*, vol. 60, no. 9, pp. 4147–4155, Sep. 2013, doi: 10.1109/tie.2013.2245615.

[48] D. Roger, S. Ait-Amar, and E. Napieralska, "A method to reduce partial discharges in motor windings fed by PWM inverter," *Open Phys.*, vol. 16, no. 1, pp. 599–604, Oct. 2018, doi: 10.1515/phys-2018-0078.

[49] L. Benmamas, "Contribution to partial discharge analysis in inverter-fed motor windings for automotive application," presented at the IEEE Elect. Insul. Conf. (EIC), 2017, pp. 348–351, doi: 10.1109/EIC.2017.8004701.

[50] L. Lusuardi, A. Cavallini, M. G. De La Calle, J. M. Martinez-Tarifa, and G. Robles, "Insulation design of low voltage electrical motors fed by PWM inverters," *IEEE Electr. Insul. Mag.*, vol. 35, no. 3, pp. 7–15, May 2019, doi: 10.1109/mei.2019.8689431.

[51] M. Szczepanski, D. Malee, P. Maussion, B. Petitgas, and P. Manfé, "Prediction of the lifespan of enameled wires used in low voltage inverter-fed motors by using the design of experiments (DoE)," presented at the IEEE Ind. Appl. Soc. Annu. Meeting (IAS), Jan. 2017, pp. 1–6, doi: 10.1109/IAS.2017.8101798.

[52] M. Szczepanski, D. Malee, P. Maussion, B. Petitgas, and P. Manfé, "Use of design of experiments (DoE) predictive models as a method of comparison of enameled wires used in low voltage inverter-fed motors," presented at the IEEE Ind. Appl. Soc. Annu. Meeting (IAS), Sep. 2018, doi: 10.1109/IAS.2018.8544548.

[53] C. Zhou, G. Liang, and A. Gu, "Fabrication of variable frequency motors using polyester-imide-hybridized resins and hyperbranched polysiloxane coated nano-TiO_2," *J. Mater. Sci.*, vol. 50, no. 22, pp. 7314–7325, Nov. 2015, doi: 10.1007/s10853-015-9288-2.

[54] P. Mancinelli, S. Stagnitta, and A. Cavallini, "Qualification of hairpin motors insulation for automotive applications," *IEEE Trans. Ind. Appl.*, vol. 53, no. 3, pp. 3110–3118, May 2017, doi: 10.1109/tia.2016.2619670.

[55] G. C. Montanari, "Characterizing insulation systems of rotating machines controlled by power electronics: The role of partial discharges," Presented at the IEEE Int. Conf. Properties Appl. Dielectric Mater., Oct. 2015, pp. 15–21, doi: 10.1109/ICPADM.2015.7295199.

[56] J. M. Martínez-Tarifa, J. Sanz-Feito, and H. Amarís, "Reduction of electrical stresses on low-voltage induction motor insulation systems through remote-controlled inverters," *Electric Power Compon.and Syst.*, vol. 36, no. 9, pp. 885–896, Aug. 2008, doi: 10.1080/15325000801960515.

[57] T. J. A. Hammarstrom, "Partial discharge characteristics within motor insulatioi exposed to multi-level PWM waveforms," *IEEE Trans. Dielectr. Electr. Insul.*, vol. 25, no. 2, pp. 559–567, Apr. 2018, doi: 10.1109/tdei.2017.006994.

[58] G. C. Montanari, F. Negri, and F. Ciani, "Partial discharge and life behavior of rotating machine wire insulation under PWM waveforms: The influence of inverter characteristics," presented at the IEEE Elect. Insul. Conf. (EIC), 2017, pp. 161–164, doi: 10.1109/EIC.2017.8004619.

[59] S. Lee and K. Nam, "An overvoltage suppression scheme for AC motor drives using a half DC-link voltage level at each PWM transition," *IEEE Trans. Ind. Electron.*, vol. 49, no. 3, pp. 549–557, Jun. 2002, doi: 10.1109/tie.2002.1005379.

[60] B. Taghia, B. Cougo, H. Piquet, D. Malec, A. Belinger, and J.-P. Carayon, "Overvoltage at motor terminals in SiC-based PWM drives," *Math. Comput. Simul.*, vol. 158, pp. 264–280, Apr. 2019, doi: 10.1016/j.matcom.2018.09.009.

[61] G. Taguchi, S. Chowdhury, W. Yuin, and N. Yuin, "Design of experiments," in *Taguchi's Quality Engineering Handbook*. Hoboken, NJ, USA: Wiley, 2005, ch. 10, pp. 501–629, doi: 10.1002/9780470258354.

[62] L.-Y. Deng, A. S. Hedayat, N. J. A. Sloane, and J. Stufken, "Statistical application of orthogonal arrays," in *Orthogonal Arrays: Theory and Applications*. New York, NY, USA: Springer-Verlag, 2012, ch. 11, pp. 247–315, doi: 10.1007/978-1-4612-1478-6.

[63] M. Jenko. *7-Files-Appendix*. Accessed: Dec. 31, 2019. [Online]. Available: http://193.2.0.110/~project/insulation/7-files-appendix.zip

[64] P. Wang, J. Li, J. Wang, A. Cavallini, and J. Zhang, "A high voltage repetitive square wave voltage generator used for endurance evaluation of inverter-fed motors," presented at the Int. Symp. Elect. Insulating Mater., vol. 1, 2017, pp. 411–414, doi: 10.23919/iseim.2017.8088772.

[65] J. Wang, P. Wang, W. Wang, K. Zhou, Q. Zhou, Y. Lei, and A. Cavallini, "Novel repetitive square wave voltage generator used for the insulation evaluation of rotating machines driven by power electronics," *IEEE Trans. Dielectr. Electr. Insul.*, vol. 24, no. 4, pp. 2041–2049, 2017, doi: 10.1109/tdei.2017.006242.

[66] N. Yanaze, M. Kozako, M. Hikita, K. Tomizawa, and M. Ohya, "Partial discharge inception voltage and breakdown voltage of micro cellular resin," presented at the Annu. Rep. Conf. Elect. Insul. Dielectric Phenomena (CEIDP), Dec. 2015, pp. 370–373, doi: 10.1109/CEIDP.2015.7351985.
[67] A. Detela and G. Lampic, "Compact multiphase wave winding of a high specific torque electric machine," U.S. Patent 9 601 957 B2, Mar. 21, 2017.

BLAZ STEFE (Member, IEEE) received the M.Sc. M.E. degree from the University of Ljubljana, in 2011. He is currently pursuing the Ph.D. degree.

He started his career at the Elaphe Propulsion Technologies Ltd., Ljubljana, where he has been promoted to a Head of industrialization, in 2017. Since then, he has been managing production and validation of in-wheel motor propulsion systems at Hangzhou APG-Elaphe Propulsion Technologies Company, Ltd., China. He became interested in production optimization while he was a Visiting Student with the Technical University of Munich. He is a part time mentor at Innovation Workshops at the Skoltech—Skolkovo Institute of Science and Technology, Moscow. His current research is focused on in-wheel electric motor optimization for production.

MARJAN JENKO (Member, IEEE) received the M.Sc. E.E. degree from the University of Ljubljana, in 1987, and the Ph.D. E.E. degree from Boston University, Boston, in 1994.

He started his career at the Iskra Microelectronics Division in Ljubljana. A year after becoming the Head of the IC Design Department, he went to Boston to pursue the Ph.D. studies. After his studies, he joined RF Power Products Inc., Voorhees, NJ, as a Research Engineer. Later, he joined System Chip, Los Gatos, CA, as a VLSI Designer. He has been with the University of Ljubljana, since 2000. He has been teaching electric circuit theory and programming engineering for the last ten years. He has been developing multi discipline projects for the education of engineering, IT, and product design students. His current work encompasses the design and optimization of product and manufacturing parameters for robust production of in-wheel electric motors. His research fields include embedded systems, control theory, distributed applications for management and control, methods of design for robust production, algorithms for process simulation, and technical education.

Dr. Jenko received two golden awards for industrial innovation from the Chamber of Commerce and Industry of Slovenia, in 2003 and 2005, where he received a silver award for an industrial innovation, in 2014.